Recent trends on semiconductors-based Z-scheme materials for photoelectrochemical water splitting

Dasari Ayodhya
Department of Chemistry, University College of Science
Osmania University,
Hyderabad-500007, Telangana State, India
*Corresponding author e-mail: ayodhyadasari@gmail.com, ayodyadasari@osmania.ac.in

ABSTRACT

Photoelectrochemical (PEC) water splitting is among the most promising approaches for a potentially clean and renewable source for hydrogen fuel from the splitting of water into hydrogen and oxygen using light source and energy conversion due to its practical efficiency. The innovative approach is the construction of a two-step photoexcitation system, often called a Z-scheme photocatalysis system, which mimics natural photosynthesis. The PEC splitting of water using various Z-scheme materials is initiated by the direct absorption of a photon, which creates separated electrons and holes in the energy band gap of the material. A Z-scheme system employs two photocatalysts, one producing H_2 and the other O_2, usually with the aid of an electron shuttle. This chapter focuses on the current state of research on nanoscale-enhanced Z-scheme photocatalyst materials for the water splitting reaction. Additionally, the recent advances achieved in especially metal oxides, metal sulfides, g-C_3N_4, and semiconductors based Z-scheme materials as photocatalyst systems for the water splitting, are also covered.

Keywords–Z-scheme materials, Photoelectrochemical systems, Water splitting, H_2 generation, Semiconductors, Reaction mechanism

Contents

I. INTRODUCTION

The water splitting is likely to play an important role in prospective sustainable-energy societies because chemical energy is storable, transportable, and can be efficiently converted into electricity using fuel cells whenever necessary. Hence, PEC water splitting may play a central role in hydrogen-based energy economies of the future [1]. To achieve successful water splitting, the charge separation in the photoelectrodes and the redox reactions (water oxidation and reduction) on the surface of the electrodes must proceed within the lifetimes of photoexcited carriers with minimized recombination [1]. Furthermore, it is of the extreme fundamental and technological importance that the photoelectrodes and photocatalysts employed in PEC water splitting are made using earth-abundant materials.

Among various alternative energies, hydrogen has been considered as a promising candidate to solve aforementioned problems because it is a source of green and renewable energy. There are a variety of strategies for hydrogen production, such as electrolysis, thermal water splitting, cracking of petroleum, hydrocarbon reforming, etc. However, these techniques are either costly or rely on fossil fuels. In 1972, Fukushima and Honda discovered PEC water splitting in which hydrogen and oxygen were released, respectively, from titanium dioxide (TiO_2) photoelectrode and platinum (Pt) counter electrode under ultraviolet (UV) light irradiation [2], revealing the potential of solar energy water splitting to produce sustainable hydrogen. This discovery stimulated great interest to explore effective photoelectrode materials for solar energy hydrogen generation via solar energy water splitting which is not only a clean process but also stores solar energy in hydrogen [3-5]. However, the widespread application of PEC water splitting still demands great efforts in the discovery of effective photocatalysts and coating process.

The photocatalytic and photoelectrochemical water splitting under irradiation by light has received much attention for production of renewable hydrogen from water on a large scale. In comparison with photocatalytic water splitting using heterogeneous powder semiconductors, PEC water splitting possesses great advantages in (i) the external or self-bias voltage can suppress recombination of photogenerated charge carriers and thus improve the separation and transfer of excited electron–hole pairs of the photocatalysts; (ii) hydrogen and oxygen can be easily separated via collection at different photoelectrodes; (iii) semiconductor films are coated on the conductive substrates, which favors scale up for industrial application in the future; and (iv) last, but not the least, it does not need stirring, so it consumes less power relative to powder photocatalytic water splitting systems [3, 6].

In practice, the performance of PEC water splitting system is dominated by the properties of the semiconductor photocatalysts that harvest solar energy for hydrogen generation. Various effective UV-light-responsive and visible-light-driven metal oxide, metal sulfide and oxynitride semiconductor photocatalysts have been well established for water splitting [7]. In the recent decades, designing visible-light-driven photocatalysts for water splitting represents a major mission for photocatalytic water splitting to maximize the solar energy conversion and storage. For instance, the metal sulfides have been found as a class of efficient photocatalysts but require sacrificial agents to reduce photocorrosion [8] and oxynitride semiconductor photocatalysts can respond to short-wavelength visible light with rather low solar energy conversion efficiency [9]. Fortunately, the hybrid photocatalyst systems have demonstrated enhanced water splitting efficiency, which, however, require dedicated design and alignment of the corresponding photocatalytic materials [7]. This chapter intensively covers the fundamental aspects of PEC water splitting using Z-scheme materials including metal oxides, metal chalcogenides, g-C_3N_4, and semiconductors under light.

II. PHOTOELECTROCHEMICAL WATER SPLITTING IMPORTANCE

The significant importance of PEC water splitting is to facilitate the transition to a hydrogen economy; hydrogen production using renewable energy is an important focus of attention. PEC hydrogen production is often dubbed ‘‘artificial photo-synthesis’’; but the techno-economic reality is that PEC must significantly outperform natural photosynthesis to become a viable commercial process for hydrogen production. While solar-to-hydrogen conversion efficiencies up to 18% have been demonstrated in the laboratory based on a spectrum of particle, thin-film and crystalline semiconductor material systems, STH efficiencies > 20% or even > 30% may be needed to compete with other renewable hydrogen technologies. Such high efficiencies are theoretically achievable, but fundamental scientific and engineering challenges remain. Inspired both by the great promise and the significant challenges, the researchers or scientists were developed several methods for the water splitting to produce hydrogen fuel.

The water splitting reaction is an uphill reaction in which the Gibbs free energy increases by 237 kJ mol^{-1}. The energy needed to drive PEC water splitting is provided by light. In the reaction processes of PEC water splitting, when a semiconductor absorbs photons with energies higher than its band gap energy, electrons in the valence band are excited to the conduction band. As a result, excited electrons and holes are generated in the conduction and valence bands, respectively. These photogenerated carriers can drive reduction and oxidation

reactions if the charge injections into the reactants are thermodynamically favourable. To achieve photocatalytic water splitting using a single photocatalyst, the band gap of the semiconductor must straddle the reduction and oxidation potentials of water, which are +0 and +1.23 V vs. normal hydrogen electrode (NHE), respectively, when the reactant solution is at pH = 0. This is the principle of one-step water splitting.

The splitting of water into H_2 and O_2 using solar light has drawn wide attention due to the abundance of the resources, water, and solar light. The generation and consumption of hydrogen fuel from water are an environmentally friendly method with zero carbon emission. The most important criterion is the electronic bandgap alignment of the photosensitive material with the redox potential of water. The generation of H_2 via splitting of water is of great importance in the current renewable energy scenario. To initiate water splitting without the supply of additional energy, the CB level of the semiconductor should be more negative than the water reduction potential and the VB should be more positive than the water oxidation potential. When the semiconductor absorbs energy greater than its bandgap, the electrons in the VB are excited leaving the holes behind. The photogenerated electrons and holes recombine instantaneously, releasing the energy as photons or heat, when they are not effectively separated. Thus, charge separation is a crucial factor in any photocatalytic activities. If the charges are successfully separated, they migrate to the surface of the semiconductor and participate in oxidation and reduction. Further, the thickness of the semiconductor is also important since if the diffusion length of charge carriers is smaller than the thickness of the semiconductor the carriers may recombine before they reach the surface of the semiconductor. The nano-sized catalysts can enhance the effective transportation of charges and active surface area for catalysis. To achieve further enhancement in H_2 production, co-catalysts are loaded onto semiconductors, which are believed to provide active sites and decrease the activation energy for water splitting. Noble metals such as platinum and ruthenium are considered typical co-catalysts to promote hydrogen generation although back reaction, that is, formation of water by the combination of hydrogen and oxygen, is an issue.

III. BASIC PRINCIPLES OF Z-SCHEME MATERIALS

Over the past years, the designing and investigations on the semiconductor heterostructure photocatalyst mainly include metal-doped, P-N heterojunction and Z-scheme materials. Among the numerous heterostructure photocatalysts, there are mainly two charge transfer modes. In one mode, the photogenerated electrons (e^-) transfer to one semiconductor with more positive CB minimum (CBM) while holes (h^+) transfer to one with more negative VB maximum (VBM). This mode can improve the charge-separation ability. However, it is unfavourable for the photocatalytic reaction because it leads to a lower height of reduction potential and higher height of oxidation potential. In contrast, in the other mode, known as Z-scheme mode, the photogenerated electrons in one photocatalyst (n-type semiconductor) with a lower CBM recombine with the holes in the other photocatalyst (p-type semiconductor) with a higher VBM, facilitated by the electron mediator [10]. As a result, the strong oxidative holes and strong reductive electrons are spatially separated to different semiconductors, and thus the whole system holds both the high charge-separation and strong redox ability. Because of these obvious advantages, the Z-scheme photocatalytic system has great potential to develop separation of the photo-induced electron and holes of the composition photocatalyst [10].

Inspired by the Z-scheme mechanism in natural photosynthesis, constructing a Z-scheme type photocatalyst driven by Z-scheme mechanism using two different semiconductor photocatalysts may overcome the issues of utilization of the longer-wavelength light; separation efficiency of the photogenerated charge carriers in the photocatalysts; the appropriate redox potential of the photogenerated charge carriers matching that of the reactants. According to the bandgap structures of two semiconductors (A and B), the separation processes of photoexcited electron-hole can be described in the following description. The electrons in the CB of A will migrate to the CB of B, and holes in the VB of B will migrate to the VB of A. Obviously, the recombination of photo-generated electron-hole pairs can be suppressed through a charge transfer between two semiconductors. Despite these advantages of heterojunction, the CB position of B is more positive and the VB position of A is more negative. Therefore, the charges transfer of traditional model is not favourable for oxidation-reduction reaction. However, according to a Z-scheme system, the fast combination is achieved between the electrons in the CB of B and holes in the VB of A. Namely; a typical Z-scheme system promotes electron-hole separation and enhances PEC performance.

In this schematic representation (Fig. 1), the reduction of water to hydrogen and oxidation of reduced redox mediators occur on one photocatalyst concurrently with the reduction of oxidized redox mediators and oxidation of water to oxygen on the other photocatalyst [1, 11]. The Z-scheme water splitting proceeds even in the absence of reversible redox shuttles in some cases because of the interparticle electron transfer during the physical contact between the hydrogen and oxygen evolution photocatalysts. When a semiconductor electrode is immersed in an electrolyte solution, electron transfer takes place between the semiconductor and the electrolyte solution so that the Fermi level is equilibrated with the redox potential of electrolyte solution. An electrolyte solution accepts (donates) electrons from (to) a semiconductor when the Fermi level of the semiconductor is

more negative (positive) than the reduction potential of the electrolyte solution. Since the density of electrons in a semiconductor is finite and the potentials of the band positions at the interfaces can be assumed to be pinned, the electron transfer causes band bending. Note that band bending could also occur in semiconductor particles suspended in an aqueous solution, although its effect might be less pronounced for nanoparticles in which the width of the space charge layer could be larger than the particle sizes. The electric field induced by the space charge layer plays an important role in charge separation. In electrodes of n-type semiconductors, which act as photoanodes, photoexcited holes accumulate on the surface of the semiconductor and are consumed in oxidation reactions, while electrons are transferred to a counter electrode via the back contact and an external circuit, and used in reduction reactions. The top of the valence band must be more positive than the oxygen evolution potential to allow a photoanode to generate oxygen. On the other hand, a p-type semiconductor works as a photocathode for hydrogen evolution when the conduction band edge is more negative than the hydrogen evolution potential.

Accordingly, PEC reactions on photoelectrodes are driven by photoexcited minority carriers in both cases. The potential of electrons on the counter electrode is identical to the Fermi level of the photoelectrode under photoexcitation. An external voltage can be applied between a photoelectrode and a counter electrode to compensate for the potential deficiency in order to drive redox reactions on a counter electrode even if the Fermi level of the photoelectrode is positioned at an undesirable potential. In such a case, the external power input, which is the product of the current and the applied voltage, should be subtracted from the energy output when the energy conversion efficiency is considered. Alternatively, a photoanode and a photocathode can be connected in tandem as in Z-scheme water splitting instead of using a single photoelectrode and a counter electrode. In the tandem configuration, the maximum photocurrent and the working potential of the photoelectrodes are theoretically determined by the intersection of the steady current-potential curves of the respective photoelectrodes.

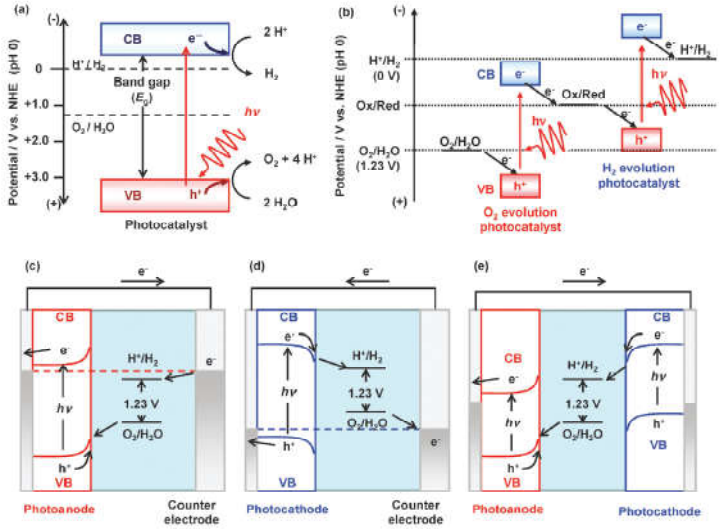

Figure 1: Energy diagrams of photocatalytic water splitting based on (a) one-step excitation and (b) two-step excitation (Z-scheme); and PEC water splitting using (c) a photoanode, (d) photocathode, and (e) photoanode and photocathode in tandem configuration. The band gaps are depicted smaller in (b) and (e) to emphasize that semiconductor with a narrow band gap can be employed [1]

IV. CLASSIFICATION OF Z-SCHEME PHOTOCATALYST MATERIALS

An artificial Z-scheme photocatalyst, inspired by the natural photosynthesis process, has greater potential in achieving high photocatalytic performance [12]. The artificial Z-scheme photocatalyst usually consists of two connected semiconductor photocatalysts: one is oxidation photocatalyst and another is reduction photocatalyst. The oxidation photocatalysts possess low VB position and exhibit strong oxidation ability, while the reduction photocatalysts usually have high CB position and display strong reduction ability. Because of the unique charge transfer as mentioned above, a Z-scheme photocatalyst with excellent photocatalytic activity possesses multiple merits, including (1) simultaneous preservation of strong reduction and oxidation abilities; (2) spatial separation of reductive and oxidative active sites; (3) high separation efficiency of photogenerated charge carriers with strong redox power; (4) a wide spectrum of photocatalysts for specific photocatalytic reactions, indicating that coupling two photocatalysts with narrower bandgaps can still meet the requirement of higher redox ability for these reactions; and (5) extended light harvesting range. Depending on the situation if the charge carrier mediator is introduced or not, and the type of the charge carrier mediator used, the Z-scheme

photocatalysts can be classified into three types: (1) traditional Z-scheme photocatalysts, where a reversible redox ion pair (such as Fe^{3+}/Fe^{2+} and IO^{3-}/I^{-}) is employed to serve as the transfer medium of charge carriers; (2) all-solid state Z-scheme photocatalysts, where an electron conductor (such as Au, Ag nanoparticles (NPs)) is used to facilitate charge carrier transfer; and (3) direct Z-scheme photocatalysts, where a direct contact between two semiconductors is ensured without any charge carrier transfer mediator and an internal electric field drives the charge carrier transfer. The historical evolution of Z-scheme photocatalysts has been presented in the previous report [17] as shown in Fig. 2(a). These three groups of Z-scheme photocatalysts exhibit distinct differences in the synthetic processes, working mechanisms, properties, and applications [12].

A. Traditional Z-scheme photocatalyst materials

A traditional Z-scheme photocatalyst was firstly reported by Bard in 1979 [13]. Since then, Z-scheme photocatalysts have attracted considerable attention. Typically, for a traditional Z-scheme photocatalyst, two different photocatalysts are coupled through an appropriate shuttle redox ion mediator. The commonly used shuttle redox ion pairs are Fe^{3+}/Fe^{2+} and IO^{3-}/I^{-}, which usually serve as electron transfer chain [12]. As shown in Fig. 2(b), when the photocatalysts are exposed to the light, the photogenerated electrons in the CB of PC II are consumed by electron acceptor species, while the photogenerated holes in the VB of PC I are consumed by the electron donor species. The photogenerated holes in the VB of PC II and the electrons in the CB of PC I with strong redox power are preserved and can participate in the oxidation and reduction reactions, respectively. Therefore, the reductive and oxidative sites are separated, resulting in the enhanced photocatalytic performance. However, traditional Z-scheme photocatalysts have some drawbacks. Namely, the redox mediator-induced back reactions are thermodynamically favored and can easily occur because the photogenerated electrons and holes with strong redox power are consumed by the shuttle redox ion pairs. In addition, light shielding effect, feasibility confined in solution systems, slow charge carrier transfer rate limited by diffusion of ion pairs, and solution pH sensitivity can also lead to the limited application of traditional Z-scheme photocatalysts. Moreover, most redox mediators are unstable and tend to deactivate, which results in a decrease in the reaction rate [12].

B. All-solid-state Z-scheme photocatalysts

While in the traditional Z-scheme photocatalysts a solution containing shuttle redox ion pairs is employed to conduct the charge transfer between both photocatalysts, an electron solid conductor is used as a charge carrier transfer bridge in all-solid-state Zscheme photocatalysts (Fig. 2(c)). The concept of all-solid state Z-scheme photocatalysts was firstly reported in 2006 for CdS and TiO_2 linked by Au as electron conductor [14]. Since then, abundant works have been published [15]. In all-solid-state Z-scheme photocatalyst systems, the selection of proper electron conductor is crucial because it can not only efficiently transfer the photogenerated charge carriers but also effectively improve the stability of the photocatalysts. Noble metals, such as Au, Ag, and Cu NPs, have been used as excellent electron mediators for constructing all-solid-state Zscheme photocatalysts [14]. In addition, other conductive materials (e.g., graphene, CNTs) are also good candidates for electron mediators [12]. It is commonly accepted that the solid conductors are much better than the aforementioned ionic redox conductors in solution, as the former are able to avoid the back reactions and make the photocatalyst recovery easy. Moreover, the all-solid-state Z-scheme photocatalysts can work both in liquid and gas phases and due to the solid conductor feature a fast charge carrier transfer. However, some noble metals serving as charge carrier transfer mediators are expensive, and the noble metal NPs may cause some problems, such as shielding effect.

C. Direct Z-scheme photocatalyst

The concept of direct Z-scheme photocatalyst was initially proposed by our group in 2013 [16]. As schematically illustrated in Fig. 2(d), two semiconductors are in close contact without charge carrier transfer mediator. In contrast to the traditional Z-scheme system (Fig. 2(b)), in the case of direct Z-scheme photocatalysts the backward reactions are significantly suppressed because of the absence of redox mediators, and the shielding effect caused by the charge carrier mediators can also be considerably reduced. Moreover, direct Z-scheme photocatalysts are resistant to corrosion.

The direct Z-scheme system exhibits a different charge-carrier migration mechanism. Here, the photogenerated electrons in PC II, which have low reduction potential, will recombine with the photogenerated holes in PC I, which have low oxidation potential. Therefore, the photogenerated electrons with high reduction potential, which are located in PC I, and the holes with high oxidation potential, located in PC II, can remain in their respective locations to achieve the spatial separation of charge carriers and optimize the redox ability of the photocatalytic system. The charge-carrier migration in the direct Z-scheme photocatalyst is physically more favorable than that in the type-II heterojunction. This is because the migration of electrons from the CB of PC II to the hole-rich VB of PC I is thermodynamically favored by the electrostatic attraction between the electrons and holes. Consequently, the direct Z-scheme system achieves superior photocatalytic performance. Note that the charge-carrier separation mechanism of the direct Z-scheme photocatalyst is similar to that of the

liquid-phase and all-solid-state Z-scheme photocatalysts, except that no redox medium is needed. Thus, the photogenerated charge carriers can directly migrate through the PC I–PC II interfaces and accelerate the charge-carrier separation efficiency of the photocatalytic system. Moreover, the absence of an expensive redox mediator greatly reduces the fabrication cost of the direct Z-scheme system. Clearly, then, this system offers three unique advantages, namely, rapid electron-hole separation efficiency, good redox ability, and low fabrication cost. With these advantages, this system shows immense potential in photocatalytic applications.

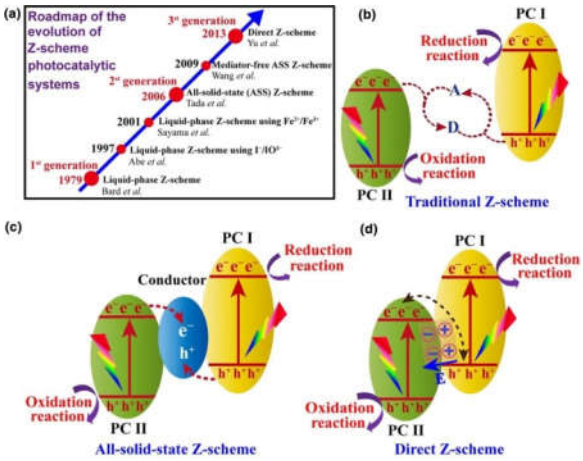

Figure 2: (a) Z-scheme photocatalyst evolution roadmap [17], (b) Schematic illustration of charge carrier transfer in traditional Z-scheme photocatalysts; A and D stand for electron acceptor and donor, respectively. (c) Schematic illustration of charge carrier transfer in all-solid-state Z-scheme photocatalysts. (d) Schematic illustration of charge carrier transfer in direct Z-scheme photocatalysts (E means the electric field) [18]

V. PRINCIPLE AND FACTORS OF PEC WATER SPLITTING

The PEC water splitting system is a two-terminal device comprised of a working electrode (WE) and a counter electrode (CE) and at least one of the electrodes is made of the semiconductor for photoelectrochemistry (Fig. 3) [19]. An auxiliary electrode, a reference electrode (RE), can be added in the PEC system for the diagnostic purpose or/and scientific study. The performance of the PEC system is determined by the steady state photocurrent flowing through the PEC circuit, which is ultimately controlled by the rate determining step. Unless high current flows, the PEC performance is limited by charge transfer kinetics, particularly, the electrochemical reaction rate at the semiconductor-electrolyte interfaces. Under irradiation, PEC water splitting involves important processes such as photon absorption, charge separation and the extraction of electrons and holes to the photoelectrodes for H_2 and O_2 evolution reactions.

In PEC, thermodynamically, the dissociation reaction, as shown in Eq. (1), is an uphill reaction with a positive Gibbs free energy.

$$H_2O\ (l) \rightarrow H_2\ (g) + \tfrac{1}{2}\ O_2\ (g) \quad (1)$$

The standard Gibbs free energy change (ΔG^0) of water dissociation is 238 kJ/mol or 1.23 eV. The half-cell reactions of formation of hydrogen and oxygen gas from water are shown in the equations below:

$$\text{Oxidation: } H_2O + 2h^+ \rightarrow \tfrac{1}{2}\ O_2 + 2H^+ \quad (2)$$

$$\text{Reduction: } 2H^+ + 2e^- \rightarrow H_2 \quad (3)$$

Reduction potential of H^+/H_2 is 0 V vs. standard hydrogen electrode (SHE) and oxidation potential of O_2/H_2O is 1.23 V vs. SHE.

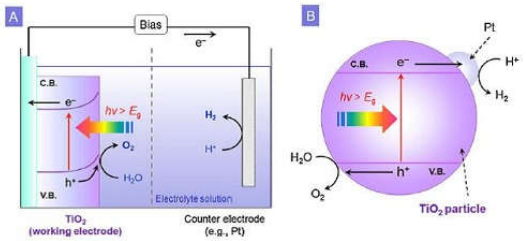

Figure 3: The schematic illustration of photoelectrochemical (a) & photocatalytic (b) water splitting [19]

Requirements of a photocatalyst

An ideal photocatalyst absorbs light irradiation, thus exciting electrons from the valence band (VB) to the conduction band (CB) while holes are created in VB. The excited electrons and holes will migrate to the surface of the catalyst. Water will be oxidized and reduced to oxygen and hydrogen gas by the photoexcited holes and electrons, respectively (Fig. 4) [20]. The process is repeated as long as irradiation of light continues. For the purpose, several fundamental requirements on the materials, which can efficiently dive the water splitting reaction upon light absorption, can be categorized. First, the photocatalyst should have an optimal band structure for maximal utilization of solar energy, which should be comparable to the photo's energy in the visible region (2.0–2.4 eV) but higher than 1.23 eV. A band gap of more than 1.23 eV is the thermodynamically required energy for water splitting, while 2.0–2.4 eV is the energy of a photon in visible light spectrum. In addition, due to energy losses from (i) loss imposed by thermodynamics due to the entropy change, and (ii) transport of electrons/holes to the surface of the photocatalyst, recombination of electron–hole pairs, kinetic losses, etc. The minimum band gap of an ideal photocatalyst should be adjusted higher. In real systems, about 0.8 eV can be allowed for global energy losses. Secondly, the bottom level of the conduction band of the photocatalyst must be more negative than the reduction potential of H^+/H_2 and the top level of the valence band should be more positive than the oxidation potential of O_2/H_2O, which allow the efficient transportation of carriers (electrons and holes) for the H_2 reduction and O_2 oxidization, respectively. Thirdly, the photo-induced electron-hole separation should be efficient and carrier mobility should be high for the efficient transportation of carriers from inside of the photocatalyst to its surface. The loss of carriers inside of the photocatalyst due to recombination definitely reduces the conversion efficiency. This requires that the materials should have high crystallinity. Fourthly, the photocatalyst should be stable in the photocatalytic reactions because the working environment is under extreme conditions, such as high temperature and strong acidic/ alkaline solutions. A number of photocatalysts (such as CdS, GaP, and TaON) exhibit suitable semiconducting properties for solar driven water splitting, but are not stable because their anions are more easily oxidized than water, resulting in fast degradation.

Finally, the photocatalyst should have high surface area and surface activity. High surface area makes the water molecules easily access the catalyst. High surface activity enables the catalyst to split water into protons and hydroxyl anions. At the same time, the possibility for the charge carrier to reach the surface increases upon decreasing the particle size (increasing surface area) of photocatalysts. Therefore, an efficient charge transport may be achieved because that the diffusion lengths of carriers may be longer than the size of the particles. The design of photocatalyst should first follow the last two fundamental requirements to find suitable candidates. Then, the electronic structures of the materials may be adjusted to satisfy the first three requirements. In addition, the high surface area of the candidates should be easily achievable.

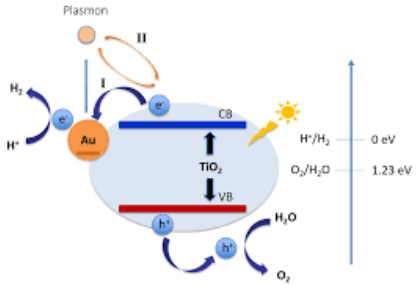

Figure 4: Band alignment to H^+/H_2 and O_2/H_2O levels [20]

VI. Z-SCHEME MATERIALS FOR PHOTOELECTROCHEMICAL WATER SPLITTING

In general, when two semiconductors with the suitable band structures were coupled into a heterojunction photocatalyst, the photogenerated electrons and holes are transferred into conduction band (CB) and valence band (VB) of the coupled semiconductor respectively because of their potential difference of CB and VB. However, the reducibility of photogenerated electrons and the oxidizability of photoexcited holes are lower after the charges transfer. Recently, the construction of biomimetic artificial Z-scheme photocatalyst has attracted more and more attention because it not only can reduce the recombination of photogeneraged electron–hole pairs, but also can retain prominent redox ability.

In natural photosynthesis system, photogenerated charges are separated and transferred between photosystem II and photosystem I through a charge transferring chain constituting the so-called Z-scheme reaction pathway. The Z-scheme photocatalytic system has greater potential to work under sunlight, as an increasing number of visible-light active H_2 and O_2 photocatalysts have been developed separately with the proper sacrificial electron donors or acceptors. Neither a H_2 photocatalyst nor an O_2 photocatalyst can function

independently to split water into H_2 and O_2. When the two are combined, however, electrons generated in the O_2 photocatalyst can be transferred to holes in the excited H_2 photocatalyst, allowing the oxidation and reduction of water to take place on the O_2 and H_2 photocatalysts, respectively. Recent development of the Z-scheme system has suggested that electron transfer between the two photocatalysts is the rate-determining process [21]. In a Z-scheme water-splitting system, an electronic mediator is used to drive the redox cycle between H_2-evolution photocatalyst and O_2-evolution photocatalyst. Therefore, the presence of an electron transporter is critical to boost effective electron relay. The redox couples are the most commonly employed electron mediators for shuttling electrons from the O_2 to the H_2 photocatalyst [22-23]. Although these ionic redox couples perform efficiently in relaying electrons, a solid electron mediator is more favorable in terms of recovery of the photocatalyst and reclamation of clean water. This is quite different from the single-step excitation photocatalyst for overall water splitting, in which the band structure of the photocatalyst must at least straddle the chemical potentials for proton reduction and water oxidation thermodynamically.

In comparison with the single photocatalyst system for photocatalytic water splitting, the advantages of the Z-scheme water-splitting system include: harvesting of a wider range of visible light using photocatalysts with narrower band gaps for H_2 or O_2 evolution, separation of H_2 and O_2 evolution on different semiconductor photocatalyst avoiding reverse reactions to a certain degree, and most importantly, much more flexibility in material screening since the proton reduction and water oxidation are separately considered on the two individual photocatalysts (Fig. 5) [24-25]. One may assemble an overall photocatalytic water-splitting system using photocatalysts which have sufficient energy only for water reduction or oxidation half reaction. For example, some metal oxides (e.g., WO_3, $BiVO_4$, ZnO, Cu_2O etc.) are generally used as water oxidation photocatalysts, but they cannot reduce H^+ to H_2 due to their more positive conduction band positions than proton reduction, however, they can be used for constructing a Z-scheme overall water splitting system. Additionally, to avoid the drawback of the soluble redox mediators in Z-scheme water splitting system, solid-state Z-scheme systems coupling two photocatalysts with solid-state mediators (e.g., Au, Ag) have been also studied.

The Z-scheme system can overcome the drawbacks of a single photocatalyst, which not only extends the light responsive range and promotes the charge separation/transfer efficiency, but also enhances the redox ability, ultimately realizing overall water splitting. In the Z-scheme water-splitting systems, another confusing issue is that the reverse reaction between photogenerated charges and soluble redox mediators suppressing the desired gas evolution. Reduction of electronic mediators competes with proton reduction reaction, and the oxidation of electronic mediators competes with O_2 evolution reaction. Such competition reactions suppress the charge utilization efficiency for overall water splitting. Taking the Fe^{3+}/Fe^{2+} mediator as an example, the reverse reactions in Z-scheme water-splitting systems include following reactions:

$$2H_2 + O_2 \rightarrow 2H_2O \quad (4)$$

$$H_2 + 2Fe^{3+} \rightarrow 2H^+ + 2Fe^{2+} \quad (5)$$

$$O_2 + 4Fe^{2+} + 4H^+ \rightarrow 2H_2O + 4Fe^{3+} \quad (6)$$

The produced H_2 and O_2 in Z-scheme water-splitting system can not only form H_2O molecule but also react with Fe^{2+} or Fe^{3+} shuttle ions in the solution. Depositing proper cocatalyst on the surface of photocatalyst is one of the useful strategies to inhibit the reverse reaction. For example, a Z-scheme photocatalyst using $SrTiO_3$:Rh and $BiVO_4$ for hydrogen and oxygen evolution, and Fe^{2+}/Fe^{3+} as electronic mediator, the effect of cocatalyst on reverse reaction was discussed [26]. The performance of overall water splitting was gradually decreased as the reaction proceeds when Pt cocatalyst was deposited on the surface of $SrTiO_3$:Rh photocatalyst, which is due to H_2O formation from the produced H_2 and O_2 as demonstrated by the significant decreases in H_2 and O_2 pressures. When Ru cocatalyst was deposited in place of Pt, the reverse reaction is inhibited almost completely, and the H_2 and O_2 evolution is maintained without obvious decrease. In control experiments, H_2 and O_2 are no longer consumed in the system after Ru cocatalyst loaded in the absence and presence of Fe^{3+} ions cases. It is a good example showing that the proper cocatalyst is important for optimizing both reduction and oxidation reactions, improving the stability and suppressing reverse reactions in Z-scheme water-splitting systems using soluble mediators.

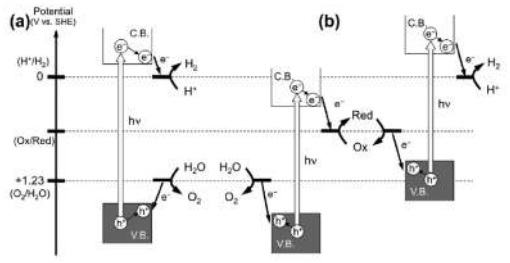

Figure 5: Schematic energy diagrams of photocatalytic water splitting systems: (a) conventional one-step system and (b) two-step photoexcitation system (Z-scheme) [25]

A. Metal oxide based Z-scheme materials

PEC cells are water electrolyzers which utilize sunlight to generate hydrogen (H_2) using semiconductor materials. They use photo sensitive anodes and cathodes to oxidize/reduce water molecules into oxygen and hydrogen gas, respectively. In order to tap most parts of the energy pertaining to the solar spectrum, heterostructured photoanodes are being developed. Further, they assist the separation of charge carriers through passivation of surface states, retain nanostructures and prevent dissolution into the electrolyte. Metal oxide semiconductors are widely used in PEC cell system for water splitting because of their photocatalytic activity and stability under irradiated aqueous conditions. The utilization of metal oxide semiconductors in PEC water splitting is a clean and economical strategy, as oxide semiconductors are inexpensive and generally very stable in aqueous solutions. However, the photochemical activity of oxide semiconductors is usually limited owing to poor charge separation and insufficient visible-light absorption, which are difficult to achieve simultaneously in a single-oxide semiconductor electrode. The slow charge transfer to solution remains the performance bottleneck, especially in complex reactions such as water oxidation and the transfer of photogenerated holes to the solution can be too slow to compete with electron-hole recombination, thus decreasing the efficiency of light-to-current conversion.

a. TiO_2

The PEC system in particular can be considered as a promising solar energy conversion technology that can directly convert solar light energy into the chemical fuel such as hydrogen through water splitting process. TiO_2-based Z-scheme photocatalysts have attracted considerable attention because of the low re-combination rate of their photogenerated electron-hole pairs and their high photocatalytic efficiency. Since Fujishima et al. [2] first reported water splitting and hydrogen generation on TiO_2 photoelectrodes, studies on semiconductor photocatalysts have entered a new era. Subsequently, the efficient stabilization of semiconductor photocatalysts has become an active area of research. In particular, the modification of TiO_2 photoelectrodes by coupling narrow band gap semiconducting materials has been considered to be one of the effective approaches in extending light absorption of the UV-light active TiO_2 photoelectrodes to the visible region. For example, one-dimensional (1D) TiO_2 nanostructures, including nanotubes and nanowires, have been extensively investigated to enhance the efficiency of hydrogen production from water by increasing the surface area as well as reducing carrier diffusion length. Its band structure is more suitable for water splitting because its conduction band is more negative than the reduction potential of H^+/H_2 and valence band is more positive than the oxidation potential of O_2/H_2O. From the given high photoactivity and chemical inertness, TiO_2 has been extensively used as an efficient photocatalyst for water splitting ever since its first utilization on PEC electrodes. However, there are several shortcomings have limited the application of TiO_2: (1) TiO_2 can only absorb UV because of the wide band gap (E_g: ~3.2 eV); (2) low quantum yield of TiO_2 due to the rapid recombination of photogenerated charge carriers; and (3) large overpotential for hydrogen production. Thus, some attempts have been made to reduce the recombination of photoinduced electron-hole pairs and to improve its utilization of solar light for TiO_2 based photoelectrodes, by modifying its crystalline structure, shape and size, doping with metals/non-metals, or coupling with other semiconductors and metals [27]. TiO_2-based Z-scheme photocatalysts achieve excellent performance in a wide range of applications, such as water splitting, CO_2 reduction, decomposition of harmful gases, and degradation of organic pollutants.

Li et al [28] designed and fabricated hierarchically branched Fe_2O_3@TiO_2 nanorod arrays (denoted as Fe_2O_3@TiO_2 BNRs) directly grown on FTO substrate as photoanode for water splitting via a simple hydrothermal growth and aqueous chemical growth process. The Z-scheme mechanism over the Fe_2O_3@TiO_2 BNRs for the enhanced PEC water splitting is proposed as follows, which is illustrated in Fig. 6, the TiO_2 and Fe_2O_3 are excited and produce photo-excited electrons and holes under solar illumination, respectively. The photogenerated holes on valance band of TiO_2 rapidly migrate to the surface and participate in the oxidation of water. Meanwhile, the photogenerated electrons from conduction band of TiO_2 recombine with holes from valance band of Fe_2O_3 at the interface contact, completing the relay of the "Z-scheme", similar to that of natural photosynthesis. As a consequence, the probability of photo-excited charge recombination can be efficiently decreased, and more photogenerated electrons on Fe_2O_3 are available to reduce H^+ to H_2, resulting in the enhanced PEC performance. Furthermore, the Fe_2O_3@TiO_2 BNRs exhibit remarkably enhanced performance for PEC water splitting, including higher photocurrent density and excellent stability, much superior to pristine Fe_2O_3 NRs. This can be attributed to the specific hierarchically branched structure, which increases surface area and improve light harvesting efficiency, as well as enhance charge transfer and separation.

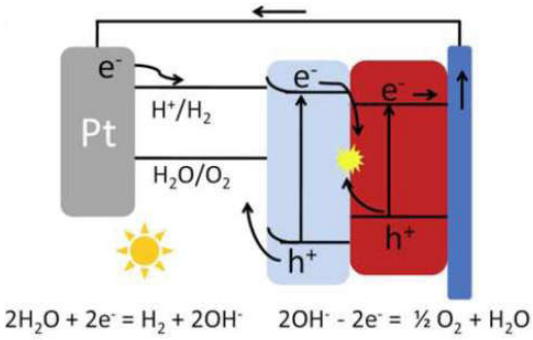

Figure 6: Schematic illustration of the charge separation and transport under solar illumination in the whole PEC cell [28]

The PEC performance of TiO_2 phtoelectrodes are enhanced with the coupling of semiconducting materials. Among the coupled semiconducting materials in TiO_2 based PEC systems, cuprous oxide (Cu_2O) is a promising candidate owing to the features of the small band gap energy of ~ 2.1 eV, a high theoretical photocurrent density of –14.7 $mA \cdot cm^{-2}$, non-toxicity, and low-cost. However, the Cu_2O layer in the photoelectrodes can easily be decomposed by photocorrosion during PEC reactions. To protect Cu_2O, $Cu_2O@TiO_2$ core-shells and Cu_2O/TiO_2 bi-layered heterojuction structures have been designed. Recently, TiO_2-1wt%$Au@TiO_2/Al_2O_3/Cu_2O$ photoelectrodes were prepared by designing an Al_2O_3 ultra-thin layer between the layer of Cu_2O and $Au@TiO_2$ using the spin-coating technique [29]. Considering the plasmonic characteristics of the $Au@TiO_2$ electrodes combining with the p-type Cu_2O photoelectrodes via the thin Al_2O_3 interface film, the heterojunctioned TiO_2-1 wt%$Au@TiO_2/Al_2O_3/Cu_2O$ photoelectrode system can be explained in terms of the charge transport property. Fig. 7 presents the mechanism and charge separation on the TiO_2-1wt%$Au@TiO_2/Al_2O_3/Cu_2O$ heterostructures photoelectrode in the PEC system. This sandwich-like photoelectrode is mimicking a Z-scheme type structure PEC cells with effective charge carrier processes. Typically, the Z-scheme provides ohmic contact as the valence band edge of p-type photocathode is close to or lower than the conduction band edge of n-type photoanode. In this Z-scheme like structure, the photogenerated electrons at the conduction band of TiO_2-1wt%$Au@TiO_2$ thin film and holes at the valence band of Cu_2O layer tend to recombine in Al_2O_3 interface layer, resulting in H_2 and O_2 evolutions driven by two separate photoelectrodes. In this case, the thin Al_2O_3 layer as an interfacial layer has the function of accelerating charge carrier separation, which subsequently leads to improved H_2 and O_2 evolution process on the electrodes. Therefore, this type of multi-layered photoelectrodes exhibits the cathodic photocurrent and charge transportation in the PEC system that differs from other TiO_2/Cu_2O systems.

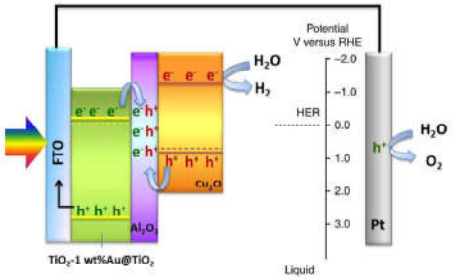

Figure 7: Schematic diagram of excitation and separation of electrons and holes on TiO_2-1wt% $Au@TiO_2/Al_2O_3/Cu_2O$ heterostructure photoelectrodes in PEC system [29]

b. WO_3

Throughout the last decade, transition-metal oxides nanostructures having uniform shape and size display highly importance in the different areas of intense scientific research and are widely used in various interesting areas such as catalysis, gas sensing, pigments in paints and ceramics, wastewater treatment, organic compounds degradation, and photocatalyst in a large variety of chemical reactions. Among different metal oxides, tungsten (VI) oxide (WO_3) is one of the most interesting semiconductor materials for the scientific community due to its low processing cost, tuneable band gap, and high solubility in aqueous solutions under acidic conditions. Also, it does not exhibits photo-corrosion activity and gives polymorphism properties. With the polymorphing nature of WO_3, it possess two important phases which attract much attention are hexagonal

phase (h-WO_3) and monoclinic phase (m-WO_3). The hexagonal phase exhibits much better interest in gas sensing and various other applications due to containing open tunnel structure and high interaction properties. On the other hand, monoclinic phase exhibits excellent photocatalytic activity under solar irradiation because it exhibits the proper band-gap energy for the adsorption of visible light.

Extensive research of WO_3, which is an n-type semiconductor, has been conducted in many applications, such as electrochromism, photocatalysis and gas sensors [30]. It is cheap, non-toxic, stable and resistant against photocorrosion in an acidic aqueous solution. Due to these properties, WO_3 has become a good semiconductor material for photoelectrode in PEC system, to produce hydrogen gas via a water splitting reaction. Researchers have been carried out to reduce the band gap of WO_3 which is approximately 2.7 eV, in order to enhance the visible light absorption and utilization [30]. However, pristine WO_3 is not effective semiconductor photocatalysts because of the low sunlight absorption, high photogenerated electron-hole recombination rate and the difficulty in H_2 evolution due to its lower position of conduction band (CB). Numerous tactics have been adopted including morphology and dimension controlling, use of hierarchical nanostructures, addition of metal and non-metal dopant and nanocomposite constructing so as to enhance the photoelectrocatalytic efficiency of semiconductor photocatalysts. Particularly, WO_3 has been used to couple with $BiVO_4$, Fe_2O_3, TiO_2 and Bi_2WO_6 to form bilayer electrodes. These bilayer electrodes have been designed for effective charge separation in order to extend the lifetime of the electron-hole pairs and hence, improve their photocatalytic activity.

Li et al [31] described g-C_3N_4-WO_3-Bi_2WO_6 double Z-scheme system was successfully prepared. The differences in band structures of g-C_3N_4, WO_3 and Bi_2WO_6 make the CB and VB levels match with each other, resulting in form a double Z-scheme system to promote charges separation and prolong the lifetime of charge carriers. The separation processes of photoexcited electron-hole in a double Z-scheme system is described in Fig. 8. Irradiated by visible light, WO_3, g-C_3N_4 and Bi_2WO_6 produce photogenerated electronhole pairs. The fast combination is achieved between the electrons in the CB of WO_3 and holes in the VB of g-C_3N_4 and electrons in the CB of g-C_3N_4 combined with the holes in the VB of Bi_2WO_6. Then the left electrons in the CB of Bi_2WO_6 can be transferred to FTO substrate. Meanwhile, the leaving holes in the VB of WO_3 participate in the oxidation reaction. As a result, a double Z-scheme system can prevent the recombination of electrons and holes leading to higher photocurrent of g-C_3N_4-WO_3-Bi_2WO_6, which is consistent with PEC result. Namely, a typical double Z-scheme system is favorable for electron-hole pair separation, resulting in the enhancement of PEC performance in g-C_3N_4-WO_3-Bi_2WO_6.

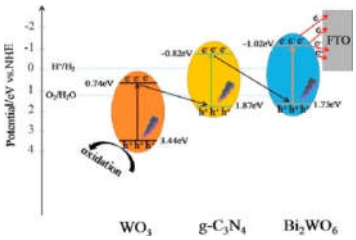

Figure 8: Double Z-scheme system schematic diagram of g-C_3N_4-WO_3-Bi_2WO_6 photoexcited electron-hole separation process [31]

Ding and Kim [32] reported 1-Dimentional WO_3@$BiVO_4$ heterojunction thin films are prepared for the first time by combining a flame vapor deposition (FVD) process with spin coating method. The PEC performance of WO_3 photoanodes and WO_3@$BiVO_4$ photoanodes were evaluated by measuring the IPCE plot in a 0.5 M H_2SO_4 solution at the applied potential of 1.0 V vs. SCE. Fig. 9 shows the IPCE plots of bare WO_3 (W_20) and WO_3@$BiVO_4$ (W_20@Bi_3) thin film photoanodes under front and back illuminations, respectively. The maximum IPCE for WO_3@$BiVO_4$ thin films under back illumination reaches up to 62.2% at wavelength of 420 nm. WO_3@$BiVO_4$ thin films under back illumination exhibit much higher IPCE than those of WO_3 thin films both under front and back illuminations and also that of WO_3@$BiVO_4$ thin films under front illumination. With addition of $BiVO_4$, light absorption edge was extended to longer wavelengths from approximately 460 nm for WO_3 to 520 nm for WO_3@$BiVO_4$ thin films due to narrower bandgap of $BiVO_4$ comparing to that of WO_3. Meanwhile, as illustrated in Fig. 10, the conduction band (CB) of $BiVO_4$ is close to the hydrogen-reduction potential and the photo-excited electrons can thermodynamically transfer from the high CB energy level of $BiVO_4$ to the more positive CB of WO_3. Holes in the valence band (VB) of WO_3 can move spontaneously to the VB of $BiVO_4$ for water oxidation. The bandgap difference between WO_3 and $BiVO_4$ also enhance the charge separation and reduces the charge recombination rate in the bulk. As a result, the WO_3@$BiVO_4$ thin films exhibit much better PEC performance than that of bare WO_3 thin films. For the case of bare WO_3 thin films, IPCE measured under front illumination is higher than that under back illumination, because light can be harvested by WO_3 thin film more efficiently when light directly illuminates toward it

compared to back illumination. The impact of light absorption (and/or reflection) by FTO-coated glass is the key factor in reducing IPCE of WO_3 thin film under back illumination. However, the IPCE for WO_3@$BiVO_4$ thin films under back illumination is far larger than that measured under front illumination for the entire range of wavelength. For the case of WO_3@$BiVO_4$ thin films, photogenerated electrons in $BiVO_4$ have to travel through the WO_3@$BiVO_4$ heterojunctional interface, which could be considered as the bottleneck for electron transport from bulk to FTO layer. Under front illumination, a large portion of light could be absorbed by $BiVO_4$ which is covering the surface of WO_3 NWs. However, charge transport rate through the $BiVO_4$ layer and WO_3@$BiVO_4$ interface was limited and, thus, low current density could be obtained. For the same reason, WO_3@$BiVO_4$ thin film didn't show the higher IPCE than bare WO3 thin film under front illumination in the short wavelength range (< 460 nm). When it was under back illumination, light in short wavelength range (< 460 nm) could be firstly absorbed by WO_3 which was close to FTO layer and the transmitted light with longer wavelength range (< 520 nm) through WO_3 could be then absorbed by $BiVO_4$. In this way, not only light could be efficiently absorbed but also charge transport was facilitated from $BiVO_4$ layer through WO_3@$BiVO_4$ heterojunctional interface and WO_3 bulk to charge collector eventually. Besides, $BiVO_4$ is usually characterized by slow water-oxidation kinetics, which has been found to be a critical limiting factor for its PEC performance. The thin films under back illumination are directly facing toward the counter electrode and the protons generated would travel shorter distance to reach counter electrode, which can also promote water oxidation rate at the interface of photoanode and electrolyte solution. Thus, WO_3@$BiVO_4$ thin films under back illumination exhibited higher IPCE than that under front illumination.

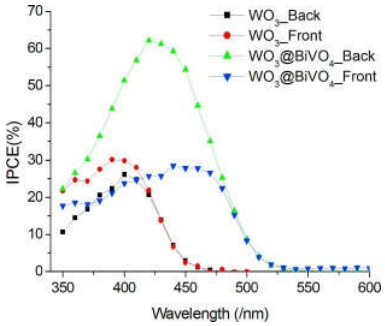

Figure 9: IPCE plots of bare WO_3 (W 20) and WO_3@$BiVO_4$ thin films (W 20@Bi 3) measured at applied bias of 1.0 V vs. SCE in 0.5 M H_2SO_4 solution under front and back illumination, respectively [32]

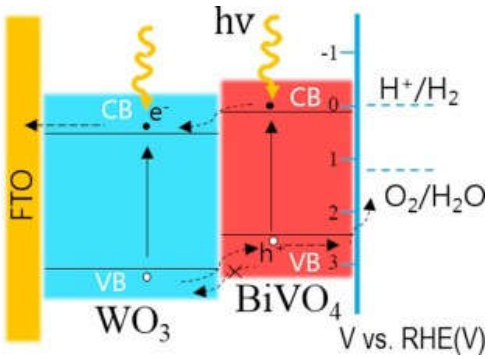

Figure 10: Depiction of energy band diagram of the 1-D WO_3@$BiVO_4$ heterojunction and charge transport process [32]

c. α-Fe_2O_3

A lot of semiconductor materials have been studied for PEC water splitting, such as TiO_2, Cu_2O, WO_3, ZnO, and α-Fe_2O_3. Among these metal oxides, α-Fe_2O_3 (Hematite) as a model material that has been received significant research attention due to its excellent optical band gap (~2.2 eV), pre-eminent chemical stability, low cost, and natural abundance. It has been predicted that α-Fe_2O_3 can attain a solar-to-hydrogen efficiency of 16.8% in theory. However, the current reported data are significantly lower than the expected value, mainly caused by its short hole diffusion length (~2-4 nm), short lifetime of photogenerated charge carriers (< 10 ps) and an obvious reduction for wavelengths approaching the band gap value in the absorption cross-section. However, the drawback of using hematite lies in its poor water oxidation reaction kinetics which requires high applied bias for oxygen evolution reaction. The other issues involved are high recombination rate of photoexcited charge carriers, short diffusion length of minority charge carriers and poor electrical conductivity.

To overcome these limitations, many efforts have been made to optimize the nanostructures of α-Fe_2O_3, for example, cauliflower-like structure, vertical nanowires and nanofilms structure were selected. Meanwhile a number of chemical techniques, including hydrothermal method, spray pyrolysis, anodic oxidation and DC magnetron sputtering, have been developed to synthesize α-Fe_2O_3 nanostructures. In addition, much essential improvement has been achieved in the photocurrent density of hematite through coupling with other semiconductors to form heterostructures, such as TiO_2/Fe_2O_3, WO_3/Fe_2O_3, $Fe_2O_3/BiVO_4$, $Fe_2O_3/ZnFe_2O_4$, n-Si/a-Fe_2O_3, p-NiO/n-Fe_2O_3 and Fe_2O_3/graphene, which have been fabricated with atomic layer deposition technique, chemical etching method, photocatalytic reduction and spin-coating approach. However, these synthetic methods are complex, expensive and difficult to control, and very few reports are available on preparation of photoelectrode by facile and low-cost process for PEC splitting of seawater. So developing a facile, safe and cost-effective method to fabricate nanostructured α-Fe_2O_3 electrodes and enhance its efficiency without altering their original morphologies is highly desired.

Li et al [33] reported a WO_3/Fe_2O_3 composite structure was innovatively proposed in this study, which was α-Fe_2O_3 nanorod arrays modified with WO_3 films. The most important part was that PEC splitting of natural seawater with α-Fe_2O_3/WO_3 NRs was reported. To investigate PEC properties of Fe_2O_3 NRs, Fe_2O_3/WO_3 NRs and WO_3 films, Linear Sweep Voltammetry (LSV) measurement was performed under 100 mW/cm^2 (AM 1.5G) illumination in an electrolyte containing 0.1 M Na_2SO_4 (pH = 6.8) at the scan rate of 10 mV/s. As a result nearly no current can be observed from pure Fe_2O_3 NRs. On the contrary, the Fe_2O_3/WO_3 NRs and WO_3 films photoanode exhibit prompt photo-response in nearly all the potential sweep range over several one-off cycles, indicating the photo-generated holes are efficiently separated and transferred to contact interface between photoanode and electrolyte, and then act for water oxidation. After coating with WO_3 films, the photocurrent of Fe_2O_3/WO_3 NRs composite photoanode begins to appear in 0.59 V vs. RHE and shows remarkable increase. Moreover, the Fe_2O_3/WO_3 NRs display the highest photocurrent density compared with others and reach a maximum value of 1.03 mA/cm^2 (1.23 V vs. RHE), which is 2.9 times as that of WO_3 films (0.36 mA/cm^2) and 50 times as that of the pristine Fe_2O_3 NRs (0.02 mA/cm^2) at the same applied voltage. The improved photocurrent density can be attributed to the introduction of WO_3. This is because the heterojunction formation between the interface of Fe_2O_3 NRs and WO_3 films, which facilitate the separation of photoinduced electrone-hole pairs.

Based on the above experimental results, a possible mechanism for the Fe_2O_3/WO_3 NRs is proposed and schematically illustrated in Fig. 11(A). According to previous works, the conduction band (CB) and valence band (VB) positions of Fe_2O_3 are about 0.55 and 2.5 eV, respectively, while those of WO_3 are 0.4 and 3.2 eV, respectively. It is well known that both Fe_2O_3 and WO_3 can produce photogenerated electrons and holes under the excitation of light. For pure Fe_2O_3 NRs, the photogenerated electrons and holes tend to recombine and only a small part of them function on the photocatalytic reaction, leading to a relatively low activity. Contrast to single phase system, the Z-scheme system was constructed between Fe_2O_3 and WO_3 in the hybrid sample, which has the advantages of promoting the separation of photogenerated charges and keeping oxidation and reduction reaction at different reaction sites. Unlike the usual structure, the formation of Z-scheme system offer an effective channel to transfer the excited electrons from the CB of WO_3 to the VB of Fe_2O_3 and caused recombination of majority carriers. Then the minority electrons further flow to the Pt counter electrode through the external circuit and consumed away for H_2 generation. At the same time, the photogenerated holes at VB of WO_3 diffuse to the contact interface between WO_3 and electrolyte for O_2 evolution. As a result, the lifetime of the minority carriers was prolonged and their reactivity was enhanced and excellent PEC performance was achieved.

Based on its good PEC performance, the Fe_2O_3/WO_3 NRs were further applied to PEC seawater splitting. As shown in Fig. 11(B) and 11(C), LSV measurement was performed in natural seawater (pH = 6.8). The photocurrent density of pure Fe_2O_3 NRs and the Fe_2O_3/WO_3 NRs were almost the same as which performed in the electrolyte containing 0.1 M Na_2SO_4. The result illustrate that the Fe_2O_3/WO_3 NRs provides the capability for sustainable development in PEC seawater splitting. For a deeper investigate of the long-term application of Fe_2O_3/WO_3 NRs photoelectrode in PEC seawater splitting, the photostability is the primary consideration. Fig. 11(D) displayed the photoresponse of Fe_2O_3/WO_3 NRs composite photoanode by photocurrent-time measurement in natural seawater at 1.23 V vs. RHE for 5 h. The initial phase of the photocurrent value is close to zero without light irradiation. When applied irradiation the photocurrent rapidly increased to about 1 mA/cm^2, and still preserved about 65% of the initial value even after 5 h of continuous irradiation (100 mW/cm^2, AM 1.5G). The exhibited high efficiency and good photostability demonstrated that the Fe_2O_3/WO_3 NRs composite photoanode is a qualified candidate for sea water splitting. The results indicated that the composited nanorod arrays exhibit higher PEC performance and enhanced stability than single-phase electrode.

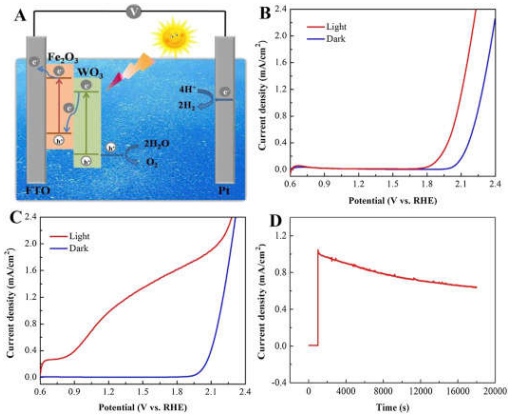

Figure 11: (A) Schematic diagram for transfer and separation of photogenerated charges and holes in the Fe_2O_3/WO_3 NRs; Photocurrent density versus potential curves for (B) Fe_2O_3 NRs and (C) Fe_2O_3/WO_3 NRs in the seawater (pH = 6.8) under illumination; (D) Photostability measurements of Fe_2O_3/WO_3 NRs in the seawater (pH = 6.8) under continuous illumination [33]

Recently, Verma et al [34] reported the Ti-doped Fe_2O_3 based photoanodes modified with MWCNTs alone and MWCNTs-Cu_2O nanopowder composites for improved photoeletrochemical performance of water splitting through Z-scheme mechanism. The Fe_2O_3 and Cu_2O, both earth abundant materials are used in functionalizing Ti doped Fe_2O_3 photoanodes with Cu_2O and MWCNTs for improving PEC performance for hydrogen generation. Pristine Ti doped Fe_2O_3 are fabricated by spray pyrolysis deposition method on the conducting ITO coated glass substrate. Two different modifications are adopted to improve the PEC performance of pristine sample by subsequent deposition of MWCNTs alone and also in combination with Cu_2O. The better photo-response in modified samples is attributed to increase in conductivity and promotion of electron transport to Fe_2O_3 layer due to presence of MWCNTs while formation of heterojunction also promotes charge transfer kinetics by effective separation of charge carriers. Offering high photocurrent density of 5.17 mA cm^{-2} at 1 V vs. SCE, high open circuit voltage (V_{oc}), least resistance, higher negative flat band potential (V_{fb}), Ti-Fe_2O_3/(MWCNTs + Cu_2O), emerges as the most photoactive sample. High applied bias photon to current conversion efficiency (ABPE) value of 4.6% is obtained for the modified sample against 0.07% ABPE for Ti-Fe_2O_3 photoanodes.

The mechanism of charge transfer in staggered type II band alignment for Fe_2O_3 and Cu_2O is shown schematically in Fig. 12. The CB for Cu_2O and Fe_2O_3 lies at −0.2 eV/NHE and 0.5 eV/NHE and VB lies at 1.8 eV/NHE and 2.4 eV/NHE respectively. This type of band arrangement is also helpful in countering the corrosion problem associated with Cu_2O. On illumination electron transfer from conduction band of Cu_2O to the low lying conduction band of Fe_2O_3 may be facilitated directly from Cu_2O or may be shuffled through MWCNTs which is acting as electron collector in Cu_2O matrix. Thus presence of MWCNTs in Cu_2O matrix helps in easy conduction of the electrons. The electrons will finally reach the Pt counter electrode through conducting ITO layer to evolve H_2 and direction of hole movement will be reverse and drift towards the photoanode/electrolyte interface for O_2 evolution. On the basis of overall performance of Ti-Fe_2O_3 was inferred that several factors are contributing towards enhanced PEC performance.

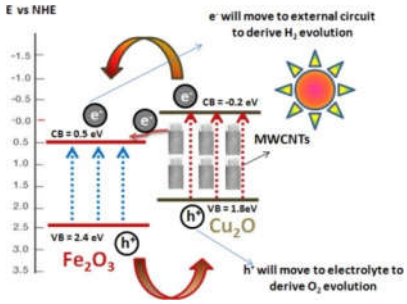

Figure 12: Schematic presentation on mechanism for charge transfer [34]

Liu et al [35] illustrated Zr-doped Ti–Nb–O nanotube arrays were prepared via electrochemical anodization and α-Fe_2O_3/Ti–Nb–Zr–O composite photoanode was fabricated by spin coating. The effects of Zr content and α-Fe_2O_3 decoration on the microstructures and photocatalytic properties of the Ti–Nb–Zr–O nanotube arrays were investigated. The charge transfer in the α-Fe_2O_3/Ti–Nb–Zr–O composite is shown in Fig.

13. As a result, the potentials of the conduction band (CB) of α-Fe_2O_3 are more negative than that of Ti–Nb–Zr–O photoanodes. Therefore, the photogenerated electrons could not transfer from CB of α-Fe_2O_3 to CB of Ti–Nb–Zr–O when the α-Fe_2O_3/Ti–Nb–Zr–O was irradiated by photon energy. However, the holes can transfer from the VB of Ti–Nb–Zr–O to the VB of α-Fe_2O_3. Additionally, holes or electrons that transfer to the α-Fe_2O_3 or Ti–Nb–Zr–O surface join in the redox reactions. Furthermore, the photogenerated electrons in the α-Fe_2O_3 and holes in the Ti–Nb–Zr–O will be transferred toward the interface α-Fe_2O_3/Ti–Nb–Zr–O to achieve the "Z-scheme" water splitting.

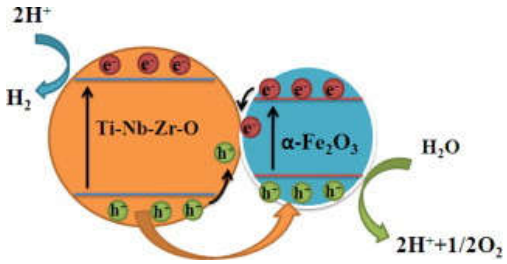

Figure 13: An energy diagram and charge transfer in the α-Fe_2O_3/Ti–Nb–Zr–O composite structure [35]

d. ZnO

Zinc oxide (ZnO) is an n-type semiconductor (E_g = 3.3 eV) with numerous idiosyncratic properties like low cost, abundance in nature, ease of synthesis, mass production, non-toxicity, anisotropic crystal structure, wide bandgap, high thermal stability, amphoteric nature, etc [36]. Among all the semiconductors, ZnO has shown the ability to mold in numerous morphologies which has lead to generation of large sets of different superstructures. Accordingly, scientific community has been taking extensive efforts to achieve different types of morphologies and orientations of ZnO superstructures. The main reason behind the growth of such morphologies is the phenomenal wurtzite (hexagonal) crystal structure of ZnO. It shows a simplified hexagonal crystal structure model depicting polar and non-polar planes of ZnO. The (0001) plane contains only Zn^{2+} ions, whereas only O_2^- ions are present on (0001) plane or vice versa. Such sequential arrangement of cations (Zn^{2+}) and anions (O_2^-) leads to a dipole moment and spontaneous polarization as well as difference in surface energies. In the same context, PEC water splitting by using semiconductor photoelectrode became popular due to its eco-friendly nature [37]. For PEC water splitting, ZnO is considered as one of the prominent semiconductor due its high efficiency and low cost. ZnO superstructures have shown astonishing results in PEC due to their exceptional physicochemical properties [38].

In PEC water splitting semiconductor photoanode is chosen by considering its band edge values. The conduction band edge of semiconductor photoanode must have higher negative potential than the reduction potential of water to generate hydrogen gas. Whereas, valence band edge must have higher positive potential than the oxidation potential of water to generate oxygen gas. Oxidation and reduction potentials of water lie exactly within the ZnO band edge potentials. Most of the n-type metal oxides own appropriate band bending for water splitting when they interact with electrolyte. Moreover, metal oxides like ZnO are considered to be more favorable for PEC water splitting than metal sulfides because they display excellent photocurrent with higher stability that too without much photocorrosion. For PEC water splitting, dye sensitized solar cells (DSSC) and photocatalytic applications the basic requirements of a photoanode material are similar and those are fulfilled by ZnO. Therefore, few reports are also available wherein ZnO is utilized for multiple applications like PEC and photocatalysis [39-40].

Recently, nanoporous $FeVO_4$ has emerged as a promising photoelctrode as anode material for PEC water splitting due to its favorable band gap (~2.06 eV), high natural abundance and superior chemical stability [41]. Comparing with solid nanofilms, nanoporous structure could not only enlarge the light absorption due to the unique light scattering effect but also facilitate the charge separation efficiency owing to the shortened charge extraction pathway. However, the high electron-hole recombination and the poor charge mobility have severely restricted the practical applications of $FeVO_4$. The construction of Z-scheme heterostructure is an efficient strategy to address these issues, which has been discussed in the introduction part. In traditional disordered Z-scheme system, it is difficult to investigate the charge transfer mechanism because of the co-existence of type-II and Z-scheme types [42]. Based on our proposed fabrication method, a pure Z-scheme system could be achieved by depositing RGO and ZnO QDs/RGO films on $FeVO_4$ substrate, in which the two semiconductors are completely separated by the electron mediator. The PEC performances of nanoporous $FeVO_4$ before and after modified with RGO/ZnO films have been explored (Fig. 14). The amperometic I-t curves in Fig. 14(a) clearly indicate that the photocurrent of $FeVO_4$/RGO/ZnO heterostructure (0.17 mA/cm^2) is more than 3 times larger than that of pure $FeVO_4$. Moreover, the PEC performance of $FeVO_4$/RGO/ZnO is also larger than the previous reported $FeVO_4$-based photoelectrodes (< 0.1 mA/cm^2) under the same bias [43]. The

LSVs examination in Fig. 14(b-d) exhibits that the construction of Z-scheme can not only enhance the photoconversion efficiency in the whole potential range, but also shift the onset potential from 0.53 V to 0.43 V, which may due to the improved charge separation efficiency of $FeVO_4$.

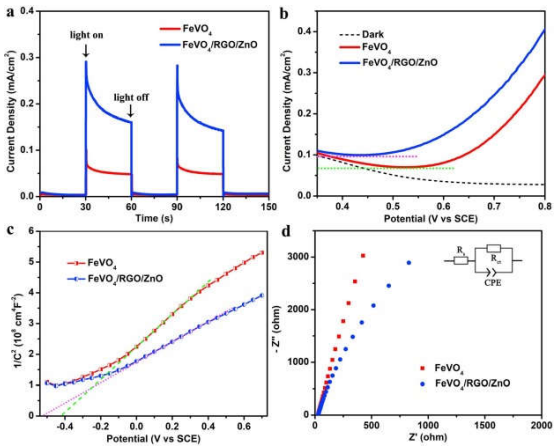

Figure 14: (a) Amperometric I-t curves at 0.6 V vs SCE and (b) linear sweep voltammograms of $FeVO_4$/RGO/ZnO heterostructures under simulated solar light. (c) Mott-Schottky plots collected at a frequency of 5 kHz and (d) Nyquist plots of the electrochemical impedance spectra of $FeVO_4$/RGO/ZnO heterostructures. The inset shows the equivalent circuit [44]

The charge transfer mechanism of $FeVO_4$/RGO/ZnO Z-scheme has been illustrated in Fig. 15. The $FeVO_4$ and ZnO are thoroughly separated by RGO films, and thus the non-Z-scheme charge transfer approaches could be restrained. It is estimated that the CB potentials of $FeVO_4$ is more negative that of ZnO, while the VB of ZnO is more positive than that of $FeVO_4$ [41]. In the Z-scheme system, RGO films act as the charge transmission bridge between $FeVO_4$ and ZnO due to its high conductivity. Under simulated solar light irradiation, the photoinduced electrons from the CB of ZnO would transfer rapidly through RGO to the VB of $FeVO_4$ and then combine with the photoexcited holes of $FeVO_4$. The left photoexcited electrons of $FeVO_4$ would migrate to the counter electrode and induce the reduction reaction while the holes of ZnO would trigger the oxidation. Obviously, the electrons transfer direction in this kind of Z-scheme, that is co-current Z-scheme, is consistent with the running direction of electrons in the external circuit. Thus, it can be known that the co-current Z-scheme could significantly enhance the charge separation efficiency and improve the PEC performances. During this process, RGO would not contribute to the generation of electrons and holes considering its low PEC activity. Furthermore, to achieve the charge transfer equilibrium, the amount of ZnO could be rationally tuned by varying the layers of ZnO QDs/RGO films. It was found that the photocurrent density of $FeVO_4$ would reach to maximum after depositing 3 layers of ZnO QDs/RGO films, and it would not increase any more even more ZnO QDs/RGO films are loaded.

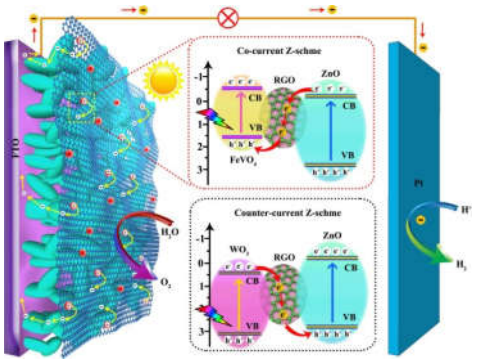

Figure 15: Schematic illustration of the charge transfer mechanism of co-current $FeVO_4$/RGO/ZnO Z-scheme and counter-current WO_3/RGO/ZnO Z-scheme systems [44]

Recently, few reports have been published to solve the absorption limit under the sunlight irradiation; various methods have been reported to extend the wavelength response of ZnO to visible region, such as coupling with CdS [45]. The CdS is regarded as the most suitable sensitizer for ZnO because of the similar lattice and narrow bandgap (2.4 eV), which could absorb more visible light and effectively separate the

photogenerated electrons and holes. On the other side, CdS can be easily obtained by chemical bath deposition method. For example, ZnO/CdS, ZnO/CdS/$ZnFe_2O_4$, ZnO/CdS/CdSe, ZnO/CdS/$CuInS_2$, and ZnO/CdS/RGO have been used as various kinds of surface modification on the photoanodes to improve the PEC performance.

Nie et al [45] reported a two-step low-temperature thermal treatment process to optimize the interface between ZnO nanorods and CdS QDs. After the thermal treatment, the PEC properties of the ZnO/CdS heterojunction show a great improvement. The improved PEC performance by the two-step low-temperature thermal treatment can also be supported by the IPCE measurement which provides a reliable method to characterize the wavelength dependent photoresponse. For a better comparison with previous results, IPCE measurements were performed in the same electrolyte at an applied voltage of 0.4 VSCE. As shown in Fig. 16(a), the IPCE value of the pristine ZnO NRs is almost negligible under visible light, but the IPCE values of the Z/C NRs with CdS QDs starts near 525 nm and increase with the wavelength decreasing which coincides with the onset of light absorption. This indicates that CdS QDs are the main absorption layer on the Z/C NRs while ZnO acts as the conductor in visible region. The IPCE of the Z/30C-150/250 NRs can reach the highest value about 95% at 350 nm, indicating 35% improvements comparing with that the Z/30C NRs (70.5%). This significant enhancement could be attributed to the optimized interface between ZnO and CdS via the two step low temperature treatment. Fig. 16(b) displays a schematic diagram of PEC water splitting using ZnO/CdS photoanode. Under light illumination, plenty of electrons are photogenerated in CdS and then thermodynamically transferred to ZnO NRs because of the more negative conduction band of CdS QDs. The electrons are further shuttled to the Pt counter electrode and react with water to generate hydrogen. The holes move to the surface of photoanode to oxidize sulfide ions [46].

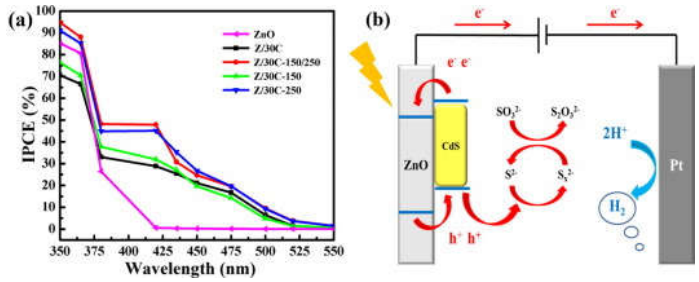

Figure 16: (a) IPCE spectra for ZnO NRs, Z/30C NRs, Z/30C-150/250 NRs, Z/30C-150 NRs and Z/30C-250 NRs and (b) The schematic diagram of photoelectrochemical water splitting with ZnO/CdS photoanode [45]

e. Cu_2O

PEC technique provides an effective method using abundant and clean solar light with a wide range of potential applications in elimination of pollution and production of energy with various unitary materials, binary materials and ternary composites have been widely used in water splitting, pollutant degradation, carbon dioxide reduction and other applications, including TiO_2, Bi_2O_3, graphene, CdS, Cu_2O and Ta_3N_5. However, still more attempt is needed to develop combination of Cu_2O with other semiconductors is highly efficient and stable photocatalytic material for energy and environmental application. Cuprous oxide (Cu_2O) is an attractive p-type semiconductor for photoelectrochemical hydrogen production with a direct bandgap of 2.0 eV and a corresponding theoretical photocurrent of 14.7 mA cm^{-2} and a light-to-hydrogen conversion efficiency of 18% based on the AM1.5 spectrum since Cu_2O possesses favourable energy band positions, high photoactivity, natural abundance of copper and its low cost production with the conduction band lying 0.7 V negative of the hydrogen evolution potential and the valence band lying just positive of the oxygen evolution potential [47]. Due to its suitable bandgap energy (2.0-2.2 eV) and more energetic conduction band (–1.0 eV), the Cu_2O has been broad used as photocatalyst in degradation of organic pollutants, solar water splitting, solar cells and PEC sensor.

Cong et al [48] demonstrated a ternary Fe_2O_3-MoS_2-Cu_2O nanocomposites were fabricated via electro-deposition and hydrothermal method, here MoS_2 as a solid-state electron mediator, n-type α-Fe_2O_3 and p-type Cu_2O as components to fabricate efficient Z-scheme ternary composites for refractory pollutants treatment. The Cu_2O is earth abundant, low-cost and has good visible light absorption with the bandgap of 2.05 eV, which makes it suitable for solar driven environment protection and water splitting. MoS_2 and Cu_2O were deposited onto the surface of α-Fe_2O_3 by simple hydrothermal and electrophoretic deposition method. The generation, separation and transfer of photogenerated charges were systematically studied. The high charge separation efficiency and strong oxidation ability were simultaneously achieved via Z-scheme transfer (Fig. 17).

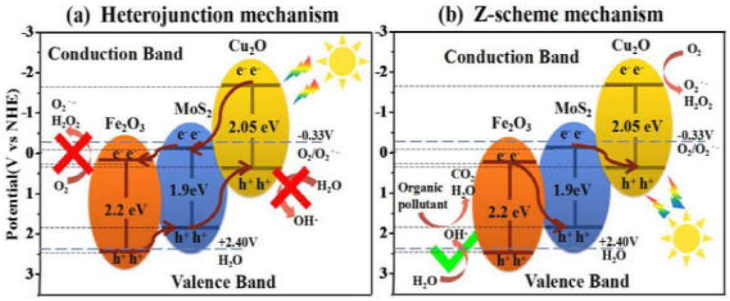

Figure 17: Proposed mechanism of charge transfer in Fe_2O_3-MoS_2-Cu_2O under visible light (a) Heterojunction mechanism and (b) Z-scheme mechanism [48]

Yoon et al [49] reported a photovoltaic-photoelectrochemical (PV-PEC) cell by integrating p-n Cu_2O thin films and ZnO nanorods (NRs) on conductive oxide substrates for water splitting through Z-scheme band structures. By comparing the photoresponses of ZnO NRs/Au/n-Cu_2O and ZnO NRs/Au/p-n Cu_2O, we could elucidate the effect of the built-in potential on PEC properties by p-n Cu_2O. ZnO NRs/Au/p-n Cu_2O showed the onset potential of 0.330 V which is more cathodic by 0.167 V than ZnO NRs/Au/n-Cu_2O. Also, its photocurrent was 0.206 mA/cm^2 under 0.2 V vs. SCE, which is 237% higher than that of ZnO NRs/Au/n-Cu_2O. These enhancements are attributed to the internal electric field by the p-n junction and the efficient charge separation and migration by utilizing both the p-n junction and the Z-scheme. In order to demonstrate the working mechanism of the system as a PV-PEC cell, the band structures of ZnO-n and ZnO-pn were illustrated in Fig. 18 based on the calculated Fermi levels of Cu_2O and the reference data [50].

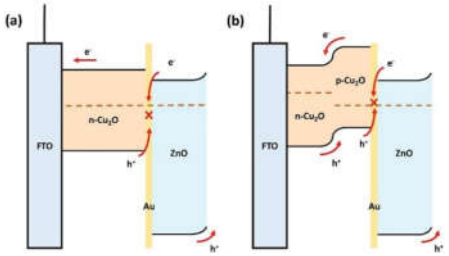

Figure 18: Schematic diagrams showing proposed energy band structures of (a) ZnO-n and (b) ZnO-pn [50]

Based upon the band diagram, the reason for the higher performance of ZnO-pn can be explained in comparison to ZnO-n. First, additional bias is obtained owing to the built-in potential in p-n Cu_2O junction. This internal potential result in higher photovoltage compared to ZnO-n. The enhanced photovoltage could be expressed as the cathodic shift in the photocurrent onset potential and the increased photocurrent. The photogenerated electrons in p-n Cu_2O with high reduction ability and photogenerated holes in ZnO with a high oxidation potential can be utilized. Secondly, higher photovoltage could originate from the effective charge separation ability of p-n homojunction Cu_2O layers. As shown in Fig. 18, the photocurrent is measured by the electron flow rate from Cu_2O thin films mostly. In the case of only n-Cu_2O layer, the probability of recombination of electrons and holes is much higher due to the absence of band bendings. However, the formation of p-n homojunction gives sufficient band bending to promote electron and hole migration in the opposite direction. Here, the energy band structures of our system can be interpreted as a Z-scheme configuration. In a Z-scheme band structure, two semiconductors are combined and higher photovoltage is obtained from them. The holes from the semiconductor having higher valence band and the electrons from the conduction band of another semiconductor were recombining at the interface. For our PV-PEC system, Z-scheme structures can work efficiently when the photogenerated holes from Cu_2O and the photogenerated electrons from ZnO exclusively meet at the Au interface and recombine together. If the photogenerated holes from Cu_2O recombine with electrons in Cu_2O and the electrons from ZnO recombine with holes in ZnO before the migration to the Au interface, the effect of increased photovoltage from z-scheme structure might be very low. In this prospect, ZnO-n has a possibility of unwanted electron-hole recombination compared to ZnO-pn where photogenerated holes have directionality to Au film because of the internal band bending. The holes in n-Cu_2O were not affected by internal bias, while the holes in p-n Cu_2O preferentially move to Au interface as mentioned above. This could be another reason for the enhancement in performance.

Yin et al [51] illustrated an integrated solar water splitting tandem cell without external bias was designed using a FeOOH modified $TiO_2/BiVO_4$ photoanode as a photoanode and p-Cu_2O as a photocathode. An apparent photocurrent (0.37 mA/cm^2 at operating voltage of +0.36 V_{RHE}) for the tandem cell without applied bias was measured, which is corresponding to a photoconversion efficiency of 0.46%. Besides, the photocurrent of FeOOH modified $TiO_2/BiVO_4$-Cu_2O is much higher than the operating point given by pure $BiVO_4$ and Cu_2O photocathode (~0.07 mA/cm^2 at +0.42 V_{RHE}). Then we established a FeOOH modified $TiO_2/BiVO_4$-Cu_2O two-electrode system and measured the current density voltage curves under AM 1.5G illumination. The unassisted photocurrent density is 0.12 mA/cm^2 and the corresponding amounts of hydrogen and oxygen evolved by the tandem PEC cell without bias are 2.36 mmol/cm^2 and 1.09 mmol/cm^2 after testing for 2.5 h. The PEC properties of the FeOOH modified $TiO_2/BiVO_4$ photoanode were further studied to demonstrate the electrons transport process of solar water splitting.

The simplified Z-schematic diagram of $BiVO_4$-Cu_2O PEC tandem cell for overall water splitting is shown in Fig. 19. To establish a theoretical feasibility PEC tandem cell, the conduction band of photoanode ($BiVO_4$) must be lower than the valence band maximum of the selected photocathode (Cu_2O). The equilibrated Fermi energy of both photoelectrodes as the reported values can generate sufficient photopotential to overcome the required 1.23 V plus electrochemical over potentials for water splitting. A thin film of nanoporous $BiVO_4$ serves as the top electrode absorbing the red part of the solar spectrum and the electrons are excited from the valence band to conduction band. Afterwards, the water is oxidized to oxygen by the remaining valence band holes (h^+):

$$H_2O + 4\,h^+ \rightarrow O_2 + 4\,H^+ \quad (7)$$

The photo-induced electrons feed into the photocathode through the external circuit. The residual light after absorbed by $BiVO_4$ is captured by Cu_2O. The conduction-band electrons of the Cu_2O enable hydrogen to be generated.

$$4\,H^+ + 4e^- \rightarrow 2H_2 \quad (8)$$

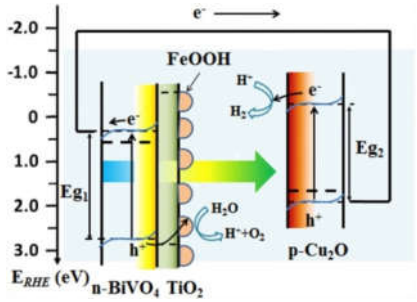

Figure 19: Simplified schematic diagram of $BiVO_4$-Cu_2O PEC tandem cell for overall water splitting [51]

The combined structure of two different semiconductor material (Cu_2O and TiO_2) are more beneficial for the electron transfer between their energy band structures and shows the improved application in various research areas. Cu_2O has been proved to be a good promoter to hybridize with TiO_2 [52] because (i) Cu_2O with a narrow band gap of 2.0 eV can extend the absorption to visible-light range with wavelength up to 620 nm; (ii) both the conduction and valence bands of Cu_2O lie higher than those of TiO_2, which is favorable for the efficient transfer of excited electrons and holes between each other. Particularly, the excited electrons of Cu_2O transfer to CB of TiO_2 and the excited holes of TiO_2 transfer to the VB of Cu_2O, respectively. This process involves a typical charge transfer mechanism of a semiconductor heterojunction. The Cu_2O/TiO_2 heterojunctions have thus shown greatly enhanced activities as compared to single TiO_2, due to the efficient charge separation between Cu_2O and TiO_2 [52]. However, it is known that the electrons in less negative CB and holes in less positive VB show weaker redox ability. Consequently, the resultant shortcoming of the typical semiconductor heterojunction is that the redox ability of transferred electrons and holes are reduced, which negatively affect the photocatalytic reactions.

Dubey et al [53] investigated the synthesis of Cu_2O nanoparticles modified vertically oriented aligned TiO_2 nanotube arrays (TNT) through wet chemical treatment of TiO_2 nanotubes and their multi-functional application as enhanced photo electrochemical and hydrogen generation through water splitting reaction. The hydrogen generation rate for aligned TNT nanostructure and Cu_2O-admixed aligned TNT nanostructure were measured in SCE under white light illumination. Fig. 20 shows the graph plotted between volumes of hydrogen produced with time. The hydrogen rate has been calculated by the volume generated in 1 h from the graph. From graph the hydrogen generation rate was found to be 78 mmol cm^{-2} h^{-1}, 110 mmol cm^{-2} h^{-1}, 158 mmol cm^{-2} h^{-1} and 129 mmol cm^{-2} h^{-1} for aligned TNT nanostructure, TNT-Cu_2O@0.1 M, TNT-Cu_2O@0.25 M, and TNT-Cu_2O@0.5 M respectively. The maximum hydrogen produced was observed in TNT-Cu_2O@0.25 M nanostructure and this may be attributed to the internal morphology of TiO_2 nanotubes changed by Cu_2O

nanoparticles because, the TNT-Cu_2O@0.25 M reveals that Cu_2O nanoparticles incorporated inside the hollow core of TiO_2 nanotubes. The other synthesized nanostructure like TNT-Cu_2O@0.1 M and TNT-Cu_2O@0.5 M also shows enhanced hydrogen production and it was relatively higher then TNT nanostructure. Thus, the improved hydrogen production in admixed Cu_2O nanoparticles on the TiO_2 surface shows the synergetic effect for higher evolution of hydrogen. Also, the obtained result indicates that the introduction of Cu_2O nanoparticles on the outer surfaces of TNT nanostructure can not only inhibit the recombination of electron-hole pairs, but also enhance the efficiency of charges transfer, which is suitable for hydrogen production by photoelectrochemical water splitting [54].

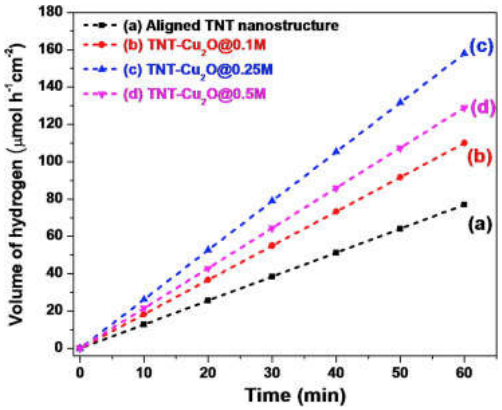

Figure 20: The hydrogen volume versus time graph for (a) aligned TNT nanostructure (b) TNT-Cu_2O@0.1 M (c) TNT-Cu_2O@0.25 M and (d) TNT-Cu_2O@0.5 M [53]

The enhanced photocurrent response of the Cu_2O modified TiO_2 nanotubes electrode in comparison to pristine aligned TNT nanostructure electrode means the electron/hole pair induced by simulated solar light gets transported more readily within the electrode material. This can be ascribed to the beneficial role of the Cu_2O nanoparticles deposited on the surface or filled inside the core of the TiO_2 nanotubes electrode. This improves the band gap as well as the charge separation and transfer performance. In other words, the unmodified aligned TNT nanostructure activated by the induced light, electrons can be excited from the valance band to conduction band, leaving the holes in the VB. However, the lifetime of the photogenerated electrons and holes is known to be very short and most of these charges will quickly recombine. Since the CB and VB of Cu_2O lie above those of TiO_2, the electrons excited to CB of Cu_2O would transfer in TiO_2. Simultaneously, the holes generated in VB in TiO_2 will prefer to transfer to that in Cu_2O Separating the electron-hole pairs in different semiconductors can induce a potential difference at the heterojunction interface, reducing the chances of electron-hole pair recombination. This will result in enhanced PEC performance (Fig. 21).

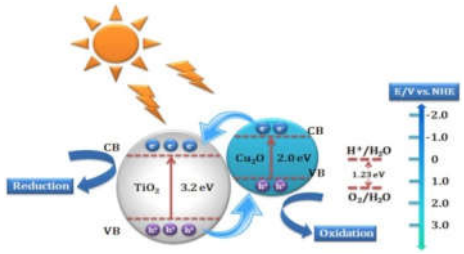

Figure 21: The schematic mechanism of the charge transfer mechanism in Cu_2O-TiO_2 system on irradiation [53]

f. $BiVO_4$

In recent two decades, bismuth vanadate ($BiVO_4$), which is an n-type semiconductor material with a band gap of 2.4 eV, has drawn increasing attention as one of the most promising photoanode materials for its capability of promoting water oxidation [55]. The $BiVO_4$ was synthesized via a solid state and melting reaction method by Roth and Waring in 1963 [56], whereas the first reported work about the use of $BiVO_4$ as photocatalyst for water splitting appeared in 1998, when Kudo et al. published their study on photocatalytic O_2 evolution on $BiVO_4$ in aqueous $AgNO_3$ solution [57]. However, poor charge separation and inefficient charge-transport properties and slow water-oxidation kinetics have been found to be key limiting factors of $BiVO_4$ for its PEC performance. So far, there is no single material which has yet been found for efficient commercial use.

Thus, many researchers have turned their interests to construct composite structures in order to counterbalance the shortages of individual components, such as $WO_3/BiVO_4/TiO_2$, $TiO_2/BiVO_4$, $WO_3@BiVO_4$, etc.

$BiVO_4$ material has been widely investigated due to the following advantages as an effective photocatalyst: 1) it is considered to be an appropriate photocatalyst material for being composed of inexpensive elements and its non-toxic properties. 2) It has band gap energy of 2.4 eV, which roughly corresponds to a light absorption cut-off wavelength at 520 nm and thus provides a good visible light responsive activity. 3) Its valence band (VB) edge located at about 2.4 eV vs. reversible hydrogen electrode (RHE) is negative enough to provide sufficient overpotential for oxygen evolution reaction, without the need of an external bias which reduces the cell efficiency. 4) The effective masses of electrons and holes in $BiVO_4$ are predicted to be much lower than other semiconductors (e.g., In_2O_3 or TiO_2), which in principle would improve the electron-hole separation and carrier extraction processes. Therefore, this makes it a promising candidate material for PEC water splitting.

In the water splitting reactions, the $BiVO_4$ has played a key role in PEC measurements. The numerous reports have confirmed that $BiVO_4$ displays high photoactivity in O_2 evolution, which is considered to be the rate-determining step for water splitting in the presence of sacrificial agent or at the aid of external bias. However, there is an obvious shortcoming for $BiVO_4$: its CB level is low and it is not energetically suitable for H_2 evolution and O_2 reduction. This issue usually leads to low photoactivity for water splitting and for degrading pollutants in nature. It is naturally expected that the feasible solution for the shortcoming is to increase the CB level of $BiVO_4$. For this, it has been demonstrated that using some elements, such as Mo and W the CB level can be changed with some success. However, this is often accompanied by new problems, involved with crystallinity decrease and carrier recombination center occurrence. When $BiVO_4$ is excited by visible light with energy higher than the bandgap, the electrons in the VB will be excited to the bottom of the CB and over the level. The excited electrons in levels higher than the bottom of the CB would possess high enough energy to induce reduction reactions. Nevertheless, the high-energy electrons usually relax to the bottom of the CB quite quickly; that is to say that the lifetimes of the produced high-energy electrons are so short that it is very difficult for them to participate in the reduction reactions. As a result, even if the UV light is used for excitation, $BiVO_4$ also displays weak charge-carrier separation, corresponding to the low photocatalytic activity. Thus, it is deduced that prolonging the lifetimes of visible-light-excited high-energy electrons is crucial to the development of efficient visible-light-response $BiVO_4$-based photocatalysts.

Zhu et al [58] reported a new artificial Z-scheme photocatalytic system has been designed herein based on the two-dimensional (2D) heterostructure of black phosphorus (BP)/$BiVO_4$. It was found that there was an effective charge separation allowing the reduction and oxidation of water to take place on the BP and $BiVO_4$, respectively. Based on the UV-visible diffuse reflectance spectra and Mott-Schottky plots, the CB and VB positions of BP and $BiVO_4$ were -0.18 and 0.52 V, 0.30 and 2.71 V vs. NHE respectively [58]. As shown in Fig. 22, the VB band of BP is very close to the CB band of $BiVO_4$. These band structures suggest a possibility of construction of the Z-scheme photocatalysis system for water splitting into H_2 and O_2. When both BP and $BiVO_4$ were excited under visible light irradiation, the photogenerated electrons in the CB of $BiVO_4$ can quickly recombine with the photogenerated holes in the VB of BP owing to their close band positions. Finally, the photogenerated electrons in the CB of BP are used for the reduction reaction, while the photogenerated holes in the VB of $BiVO_4$ are used for the oxidation reaction. Thus, the overall water splitting into H_2 and O_2 by using the BP/$BiVO_4$ composite as the photocatalyst was assessed. The optimum H_2 and O_2 production rates on BP/$BiVO_4$ were ca. 160 and 102 μmol g^{-1} h^{-1} under > 420 nm light irradiation, without using any sacrificial agents or external bias.

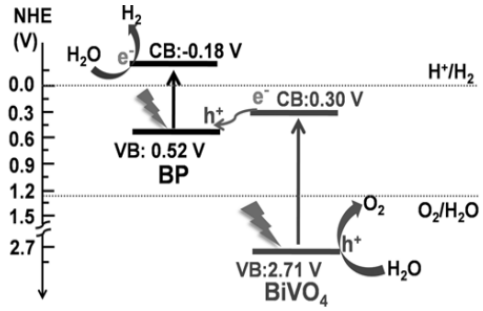

Figure 22: Schematic diagram of Z-scheme photocatalytic overall water splitting using BP/$BiVO_4$ under visible light irradiation [58]

Safaei et al [59] investigated two types of heterojunctions, comprised of g-$C_3N_4/BiVO_4$ and $TiO_2/BiVO_4$, where the former has superior efficiency. Various experimental methods have been utilized to investigate the performance of these heterojunctions. The experimental results, counterchecked with first

principle density functional theory (DFT) simulations, confirmed that g-C_3N_4/$BiVO_4$ forms a van der Waals type heterojunction (Z-scheme), where an internal electric field facilitates the separation of electron-hole pair at the g-C_3N_4/$BiVO_4$ interface which further restrains the carrier recombination. The proposed heterojunctions are illustrated in Fig. 23, where TiO_2 and $BiVO_4$ form a Type (I) heterojunction while g-C_3N_4 and $BiVO_4$ comprise Type (II) heterojunction. It is worth mentioning that the Fermi level shifts for two semiconductors when they interface one another, forming an overall band diagram (vide infra). In the present research, type (I) heterojunction for TiO_2/$BiVO_4$ and type (II) heterojunction for g-C_3N_4/$BiVO_4$ can be further extended into a Z-scheme heterojunction under the application of a positive bias. The anodic photocurrent suggests oxidation reaction at $BiVO_4$ and reduction at the counter electrode. This implies that high energy electrons of TiO_2 and g-C_3N_4 directly reduce water at the counter electrode while the electrons at the conduction band energies of $BiVO_4$ are recombined with the holes at the valence band of TiO_2 and g-C_3N_4. Furthermore, the holes at the valence band of $BiVO_4$ surface are left to oxidize water. In both aforementioned heterojunctions, TiO_2 and g-C_3N_4 act as electron extraction layers as pathways to transfer electrons to the counter electrode as opposed to other structures where g-C_3N_4 acts as hole extraction layer.

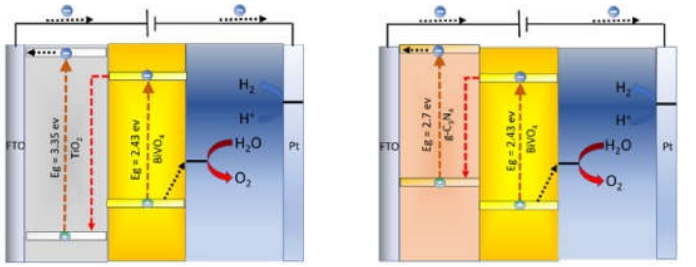

a) TiO_2/ $BiVO_4$ Type (I) heterojunction b) g-C_3N_4/ $BiVO_4$ Type (II) heterojunction

Figure 23: The band diagram of (a) TiO_2/$BiVO_4$ type (I) heterojunction and (b) g-C_3N_4/$BiVO_4$ type (II) heterojunction [59]

Soltani et al [60] reported the fabrication of p-n junctions with built-in electric field effect between n-type $BiVO_4$ (BVO) and p- type $BiFeO_3$ (BFO) can be efficient strategy to separate photogenerated carriers and enhances photocurrent density and photostability in BVO. It can be synthesized by a facile ultrasonic/hydrothermal route through BFO/BVO p-n junction that greatly improved the performance of n-type BVO and p-type BFO for photocatalytic degradation of tetracycline (TC) and photoelectrochemical (PEC) water splitting. In addition, the role of back and front side illumination on photocurrent density and carrier lifetime, particularly for the suppression of electron-hole recombination in BFO/BVO photoanodes, has not been investigated. In the present study, we report a novel ultrasonic route for the fabrication of a BFO/BVO p-n junction nanocomposite (NCs) with an extended stability in order to greatly improve the performance of n-type BVO and p-type BFO for the photocatalytic degradation of TC and PEC water splitting. The photocatalytic degradation of TC by BFO/BVO as a function of initial pH is demonstrated in comparison with that of BFO or BVO alone, and a mechanism is postulated for the greatly improved TC photodegradation by the p-n junction structure. The photocurrent density of the BFO/BVO p-n junction photoelectrodes under UV-vis light and visible light is demonstrated in comparison with that of BVO. In addition, the chemical stability and the role of the back and front side illumination on the photocurrent density of BVO and BFO/BVO are further investigated to reveal the improvement of the charge transfer in the BFO/BVO photoelectrode. The as-synthesized BFO/BVO heterostructure exhibited enhanced PEC performance and improved charge transfer due to the successful combination of BVO and BFO, which decreased the charge carrier resistance across the BVO/BFO-electrolyte interface (Fig. 24).

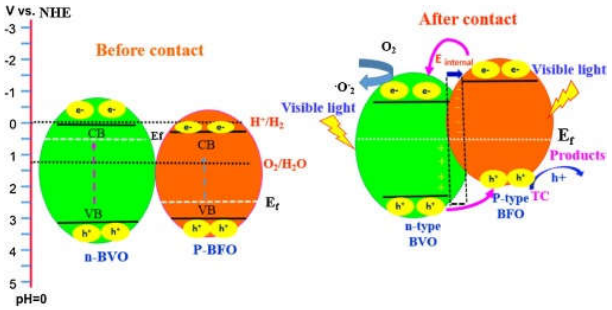

Figure 24: Highly simplified schematic diagram of the formation of a p-n junction and the possible charge-separation process for the TC photocatalytic improvement by the BFO/BVO p-n junction [60]

B. Metal sulfide based Z-scheme materials

Over the last few decades, semiconductor photocatalyst has been in widely researched into many multidisciplinary fields of materials, chemistry, environment and many others. Hundreds of semiconductor photocatalysts have been used for multifunctional applications such as hydrogen production and CO_2 reduction in energy field, along with sewage disposal and air purification in environment pollution control. Nevertheless, none of these semiconductor photocatalysts can definitely satisfy all requirements of practical applications, for instance, high utilization of solar energy, high security, high efficiency, high stability and low-cost. Various types of photocatalysts such as TiO_2, alkali metal base, ZnO, Cu_2O, $BiVO_4$, and metal sulfide base materials for increasing the amount of H_2-production from the solar water splitting have been reported since Fujishima and Honda [2]. Among those photocatalyst materials, metal sulphides are considered as a promising candidate because of their suitable band gap energy, band position, and catalytic activity.

a. ZnS

Semiconductors have been investigated as photoelectrode materials for technological solutions to environmental pollution and energy shortage. By using II-VI and III-V semiconductor materials as photoelectrodes, numerous efforts have been made in order to enhance the water splitting but most of them have shown low efficiency and/or poor stability when used alone in a PEC cell. Zinc sulfide (ZnS) is regarded as one of the most important II-VI semiconductors with wide direct band gaps (3.72 eV for the cubic zinc blende phase [61] and 3.77 eV for the hexagonal wurtzite phase [61]). For example, enhanced PEC performances using ZnS nanostructures were demonstrated in applications such as hydrogen generation from water, degradation of organic substances, and dehalogenation of halogenated benzene. Moreover, ZnS thin films or nanostructures were deposited on CdS or $Cu(In,Ga)(Se,S)_2$(CIGS) host materials as cocatalysts to suppress photocorrosion and to increase photocurrents.

Hassan et al [62] investigated the improved PEC water splitting performance of ZnS/GaN heterostructures enabled by the superior photocatalytic behavior of ZnS. We show that a film of ZnS improves the stability of GaN photoanodes by protecting the surface of GaN films from photocorrosion reactions. Additionally, we show that ZnS/GaN heterostructures can reduce the recombination rate of charge carriers owing to their type-II band alignment. The water splitting performance of ZnS/GaN photoanodes was investigated for various ZnS thicknesses and GaN doping concentrations for optimized efficiency and stability (Fig. 25).

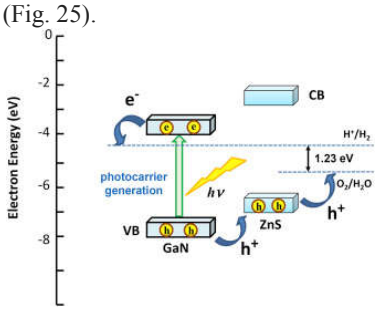

Figure 25: Schematic band diagram of a ZnS/GaN heterostructure and carrier transport during PEC water splitting, where CB and VB respectively denote the conduction and valence bands, and the horizontal dotted lines represent the redox potentials of H^+/H_2 and O_2/H_2O. Incident photons (hν) are captured to generate electrons (e^-) and holes (h^+) and the photogenerated electrons and holes that have sufficient energy drive the redox chemical reactions to split water into H_2 and O_2 [62]

Recently, Hao et al. [63] reported the ZnS/g-C_3N_4 heterostructures with abundant zinc vacancy (V_{Zn}) defects for PEC water splitting. As illustrated in Fig. 26(a), the photoluminescence (PL) emission intensity significantly decreased after coupling with ZnS. Remarkably, the V_{Zn}-rich CZV20 (g-C_3N_4/ZnS-20wt%) heterojunction showed the weakest PL intensity among all the samples, attesting the effective charge transfer between ZnS and g-C_3N_4. CZV20 heterojunction presented the maximum photocatalytic H_2 evolution rate (Fig. 26(b)), which was about 30 times greater than that of the pure g-C_3N_4 (24.09 μmol h^{-1} g^{-1}). This superior photocatalytic H_2 evolution rate was arisen from the excellent charge separation efficiency and light-absorbing capacity caused by the abundant Zn vacancies. From the linear sweep voltammetry (LSV) analysis (Fig. 26(c)-(d)), the CZV20 electrode demonstrated the highest current density, which clearly manifested the synergistic promotion of charge carriers' separation capability of ZnS/g-C_3N_4 heterojunction. More interestingly, the H_2 production activity of ZnS was originated from the two-photon excitation by the two steps of absorption mechanism (Fig. 26(e)-(f)) due to the existence of Zn vacancy defects in the band gap of ZnS. As such, these results substantiate that appropriate Zn vacancy defect is a propitious approach to ameliorate the H_2 production activity and regulate the behavior of light absorption in photocatalysis, which can be a game-changing breakthrough in energy conversion.

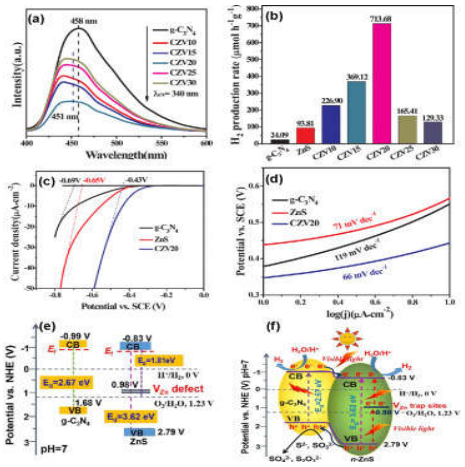

Figure 26: (a) PL spectra of the ZnS/g-C_3N_4 nanocomposite, (b) Photocatalytic H_2 production rates of g-C_3N_4, ZnS and ZnS/g-C_3N_4 photocatalysts in 0.35 M Na_2S and 0.25 M Na_2SO_3 solution under visible light ($\lambda \geq 420$ nm) irradiation. (c) LSV curves and (d) Tafel slopes for g-C_3N_4, ZnS and CZV20 samples, (e) Diagram of band structures for g-C_3N_4 and ZnS. (f) Visible-light photocatalytic mechanism for H_2 production over CZV20 nanocomposites [63]

b. CdS

Among the diverse types of semiconductor photocatalysts, cadmium sulfide (CdS) with its appropriate band gap (2.4 eV) has been investigated extensively [64]. Meanwhile, for overcoming the shortcoming of CdS such as rapid photogenerated carriers recombination and photocorrosion, many researchers have been conducted, including loading other semiconductors, such as CdS-$ZnFe_2O_4$, CdS-TiO_2, CdS-NiS, CdS-MoS_2, CdS-BiOCl-Ag_2CO_3 and CdS-MoO_3-WO_3 as binary metal oxide, own the narrow band of 2.8 eV, has attracted more and more attentions for multiple applications, such as oxygen evolution and H_2 production.

Hu et al [65] reported WO_3/CdS-DETA (diethylenetriamine) composites were successfully prepared by facile in-situ solvothermal method. DETA organic molecules were intercalated between CdS structure forming unique and stable inorganic-organic CdS-DETA NBs. Then WO_3 was constituted with as-prepared CdS-DETA to form direct Z-scheme WO_3/CdS-DETA composites. WO_3/CdS-DETA photocatalyst exhibited excellent HER performance comparing with pure WO_3 and CdS-DETA. Furthermore, the systematically calculated energy band structure and charge transfer of the WO_3/CdS-DETA using the hybrid density functional approach. This calculation revealed that the band structure of WO_3/CdS-DETA composites had significant advantages to improve photocatalytic efficiency under visible-light irradiation. This studying not only designs inorganic-organic CdS-based composite for high photocatalytic H_2 generation activity and superior stability, but proposes Z-scheme system for this novel composite.

The mechanism of photocatalytic reaction and diffusion process of photoexcited electrons and holes of the CdS/WO_3 heterostructure are illustrated in Fig. 27. Under the irradiating of visible light, electrons absorbed photon energy and then excited from VB of CdS and WO_3 to their CB. Meanwhile, the photogenerated holes were left in their VB. As mentioned above, the direction of built-in electric field is from CdS (0 0 1) surface to WO_3 (1 0 0) surface, which promotes the migration of photogenerated electrons from CB of WO_3 to VB of CdS and leads to the recombination of electrons and holes in VB of CdS. Moreover, built-in electric field also hinders the photoexcited electrons in CB of CdS to diffuse into CB of WO_3 and photoexcited holes in VB of WO_3 to diffuse into VB of CdS. Therefore, under the effect of built-in electric field, the photogenerated electrons of WO_3 and holes of CdS were consumed. As indicated in Fig. 27, the photogenerated electrons and holes naturally accumulated in CB of CdS and VB of WO_3, respectively. The separation of photoexcited charge carriers in space prolonged their lifetime and enchanced the probability of the photoexcited charge carriers participating in the photocatalystic reaction, which will greatly improve the photocatalytic activity of the WO_3/CdS heterostructure. The above analysis implied that WO_3/CdS heterostructure was a direct Z-scheme system.

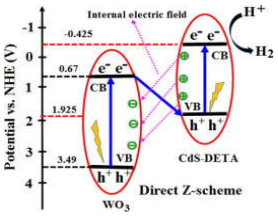

Figure 27: Proposed direct Z-scheme photocatalytic mechanism for WO_3/CdS-DETA heterostructure [65]

Li et al [66] developed sandwich heterostructure of TiO_2 nanocrystals passivated Z-schemed core-shell CdS-CdO nanorod arrays that achieved significant improvements on photo current generation as compared to plain CdS nanorod arrays. The main electrode material, CdS nanorod arrays, was grown on the surface of an FTO substrate. The one-dimensional nanostructure of the nanorod provides not only confined and directed pathways for fast charge transport, but also large surface to volume ratios to accommodate large amount of active sites for the involved electrochemical reaction to proceed. A thin CdO layer was introduced in situ to the CdS nanorod surface through controlled thermal oxidation, to form the core-shell CdS-CdO nanorod array. The suitable matching of the band structure of the two semiconductors establishes a direct Z-scheme charge transfer mechanism, effectively suppressing the recombination of the photo induced electrons and holes within the CdS domain and thus significantly enhancing the photovoltaic conversion efficiency. Further decoration of TiO_2 nanocrystals on the nanorod surfaces was achieved with a successive ionic layer absorption and reaction (SILAR) process. These TiO_2 nanocrystals passivated the surface defects and trap states of CdO to suppress the surface electron-hole recombination to further boost the photo currents. It has also been proposed that the passivating material may increase the extent of the band bending at the electrode/electrolyte interface to facilitate hole transfer to the electrolyte, advantageous to photo current generation. The sandwich heterostructure of TiO_2@CdO/CdS NR generated a high photo current density of 3.2 mA/cm^2 at 1.23 V vs. RHE, 141% higher than that by the plain CdS nanorod array electrode and 32% higher than that by the CdO/CdS nanorod array electrode. The stability of the electrode is excellent, with a photo current retention of 92% after 5 h operation.

A charge transport and transfer mechanism is proposed in Fig. 28 to explain the success of the surface modification implemented on the CdS nanorod array to boost the current densities. First, the band structure of the core-shell CdS-CdO was constructed according to the energy bandgaps and conduction band positions of CdS and CdO. The band structure is a direct Z-scheme band structure. Upon illumination, both CdS and CdO absorb optical energy and generate photo induced electrons and holes. The photo induced holes of the CdS are consumed by the photo induced electrons of the CdO at the CdO/CdS interfaces, a Z-scheme charge transfer pathway, suppressing the electron-hole recombination within the CdS domain. The photo induced electrons of the CdS can thus be effectively transported out of the anode and reach the cathode via the external circuit to reduce water for hydrogen generation. Note that it is difficult for the photo induced electrons of the CdO to diffuse to the TiO_2 domain since the conduction band position of anatase TiO_2 (0.25 V vs. RHE) is more negative than that of the CdO (0.74 V vs. RHE). Consequently, the photo induced electrons of the CdO can be effectively used to consume the photo induced holes of the CdS. As to the TiO_2 nanocrystals, they passivate the surface defects and trap states of the CdO to suppress the possible surface electron-hole recombination of the CdO. The presence of the TiO_2 nanocrystals can also cause the band bending at the CdO/TiO_2 interface to help transport photo induced holes to the electrolyte.

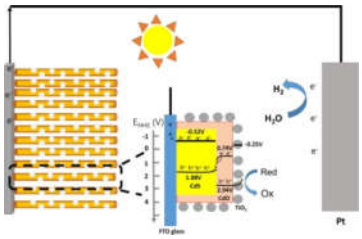

Figure 28: Band structure and charge flow of present PEC system [66]

C. g-C_3N_4 based Z-scheme materials

Carbon nitride can exist in various phases not only depending on the C to N ratio, but also on atomic arrangements. Among these phases, the graphitic carbon nitride (g-C_3N_4), a heptazine based form, is regarded to be the most stable structure, and can be realized by thermo-condensation of C/N/H-containing precursors. Wang et al. first reported that g-C_3N_4 is suitable for water splitting under visible light illumination in the presence of a sacrificial donor [67]. Recently, metal-free graphitic carbon nitride (g-C_3N_4) has attracted intensive attention for the applications in photocatalytic organic pollutant degradation, water splitting, CO_2 reduction and organic

synthesis under visible light [68]. The calculated electronic and optical properties of functionalized g-C_3N_4 nanotube evidence the narrowed band gap and optical gap, and enhanced mobility, satisfying basic prerequisites as a new class of high efficiency photocatalysts for water splitting and other avenues of solar energy utilization. In detail, g-C_3N_4 is a medium band gap (~2.7 eV) semiconductor with good visible light response (up to 460 nm) and high stability [69]. Generally, the VB position (E_{VB}) of g-C_3N_4 is about 1.57 eV, and the CB position (E_{CB}) is about −1.13 eV [70]. However, the pristine g-C_3N_4 is usually limited by unsatisfactory photocatalytic efficiency due to the insufficient visible light absorption, low surface area and the fast recombination of photoexcited electron-hole charges [71]. As mentioned above, the construction of direct Z-scheme heterojunction with matched VB and CB is benefit for enhancing the separation efficiency and promoting the redox ability. Successful cases, such as CeO_2/g-C_3N_4, TiO_2/C_3N_4, BiOI/gC_3N_4, Bi_2O_3/g-C_3N_4, WO_3/g-C_3N_4, Ag_3PO_4/g-C_3N_4, $BiVO_4$/g-C_3N_4, and so on. Nowadays, most efforts of Z-scheme photocatalysts have been devoted on binary composites. However, these binary systems were always impeded by the limited visible light response and relatively low charge separation efficiency. Recently, the fabrication of g-C_3N_4 based Z-scheme ternary composites by combing conducting materials, co-catalyst, and another semiconductor has attracted great attention as a promising approach to further enhance visible light absorption, create faster charge carrier separation and facilitate effective redox reactions.

Jiang et al reported [72] and proposed the mechanism of novel direct solid state dual Z-scheme WO_3/g-C_3N_4/Bi_2O_3 was successfully synthesized by one step co-calcination strategy. The obtained WO_3/g-C_3N_4/Bi_2O_3 composites exhibit more efficient photocatalytic performance for tetracycline (TC) degradation than pure g-C_3N_4, WO_3, Bi_2O_3 and their binary composites under the visible light irradiation. The enhanced photocatalytic activity of WO_3/g-C_3N_4/Bi_2O_3 composite can be ascribed to improved visible light absorption, increased surface area and enhanced separation efficiency of photo-generated electron-hole pairs. According to the band gap structures of WO_3, g-C_3N_4 and Bi_2O_3, the separation processes of photoexcited electron-hole could be exhibited in Fig. 29(a-b), respectively. There are two possible charge separation ways for WO_3/g-C3N_4/Bi_2O_3 composite. In detail, one is the traditional double-transfer mechanism and the other is Z-scheme mechanism. As shown in Fig. 29(a), the electrons in the CB of g-C_3N_4 will migrate to the CB of Bi_2O_3 and then transfer to the CB of WO_3 if the charge carriers of WCB transfer according to the double-transfer mechanism, while, the holes in the VB of WO_3 will migrate to the VB of Bi_2O_3 and final transfer to the VB of g-C_3N_4. As a result, the electrons will accumulate to the CB of WO_3 and the holes will gather to the VB of g-C_3N_4. If this is true, the accumulated electrons on the CB of WO_3 cannot reduce O_2 to form % O_2^- radicals due to the CB of WO_3 is more positive than the potential of O_2/O_2^- (−0.33 eV vs. NHE). Moreover, the holes of g-C_3N_4 cannot oxidize OH^- or H_2O to give OH radicals due to the VB potential of g-C_3N_4 is lower than the standard redox potential of OH^-/OH radicals (2.40 eV vs. NHE) and H_2O/OH radical (2.72 eV vs. NHE). However, the trapping experiment and ESR results indicated that $^{\bullet}O_2^-$, h^+, and $^{\bullet}$OH are the predominant active species for the WO_3/g-C_3N_4/Bi_2O_3 photocatalytic system. Therefore, the separation and transfer process of the photogenerated electron-hole charges should not follow the common heterojunction process in Fig. 29(a).

According to the above discussion and the experimental results, a possible direct solid-state Z-scheme mechanism was proposed. As schematized in Fig. 29(b), g-C_3N_4, WO_3 and Bi_2O_3 can produce photoinduced electron-hole pairs under visible light irradiation. Then, the photoinduced electrons in the CB of WO_3 would transfer and recombine with the holes in the VB of g-C_3N_4. Simultaneously, the photogenerated electrons in the CB of Bi_2O_3 also combined with the holes in the VB of g-C_3N_4. The migration of charge carrier can result in the electron accumulating in the CB of g-C_3N_4 (-1.05 ev), and the holes retained in the VB of WO_3 (3.34 eV) and Bi_2O_3 (3.14 eV), respectively. Therefore, the photoexcited electrons that remained and accumulated in the CB of g-C_3N_4 could be trapped by O_2 to yield $^{\bullet}O_2^-$. Simultaneously, the holes left in VB of WO_3 and Bi_2O_3 have enough energy to degrade TC or oxidize H_2O to form $^{\bullet}$OH radicals. The active radical ($^{\bullet}O_2^-$ and $^{\bullet}$OH) subsequently participate in the removal of TC. Therefore, it can be concluded that the photocatalytic reaction of prepared WO_3/g-C_3N_4/Bi_2O_3 composite follows a direct solid-state Z-scheme mechanism, which not only can accelerate the separation and transfer of photogenerated charges but also can retain the strong redox ability for efficient degradation of TC.

Recently, exfoliated thin graphitic C_3N_4 nanosheets (g-C_3N_4 NS) have shown great promise in photocatalytic HER owing to their abundant reactive sites associated with the improved surface area and also the promoted charge separation by shortening the diffusion length of photoexcited electron-hole pairs within the decreased dimensions. Motivated by these results, we herein present a hierarchical g-C_3N_4-supported $CuInS_2$ (GsC) by in situ hydrothermal growth of $CuInS_2$ (CIS) on thin g-C_3N_4 NS toward Z-scheme photocatalytic water splitting. The GsC offers an intimate contact between CIS and g-C_3N_4 NS with strong couplings, suppressing the detrimental recombination of photogenerated carriers and resulting in a significant quenching in the photoluminescence (PL) of g-C_3N_4 NS to induce an over 6-fold increase in the PL lifetime. As the result, the GsC shows a high H_2 production rate up to 1290 μmol g^{-1} h^{-1} under visible light irradiation ($\lambda > 420$ nm) with an outstanding stability in hours of operation, setting a new benchmark for visible-light-driven water splitting based on CIS photocatalysts [73].

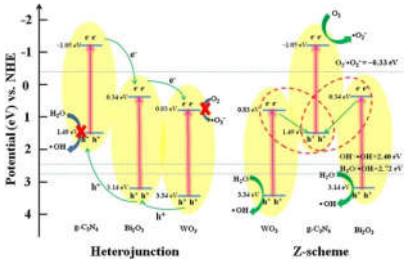

Figure 29: Schematic diagram for the possible charge separation of $WO_3/g\text{-}C_3N_4/Bi_2O_3$, (a) Heterojunction, (b) Z-scheme [72]

An energy band diagram for the GsC is thus depicted in Fig. 30, where energetically the VB of the CIS is capable to accept the photoinduced electrons from the CB of g-C_3N_4 NS and the staggered alignment of energy levels here in the GsC can provide a Z-scheme system with the right band potential for photocatalytic water splitting [74]. To rule out the energetically possible electron transfer from the CB of the CIS directly to the CB of g-C_3N_4 NS in the GsC, we performed the photodeposition of Pt nanoparticles to confirm the Z-scheme charge transfer pathway. As reported earlier, the reduction of Pt^{4+} in H_2PtCl_6 by photoinduced electrons under illumination would form Pt nanoparticles that are inclined to accumulate around electron-rich sites due to the electrophilic nature of Pt^{4+} species. The Pt nanoparticles are assembling around the CIS rather than staying randomly on the g-C_3N_4 part, implying that photoexcited electrons remain to reside on the CIS as predicted by the Z-scheme route instead of being transferred to g-C_3N_4 NS under illumination.

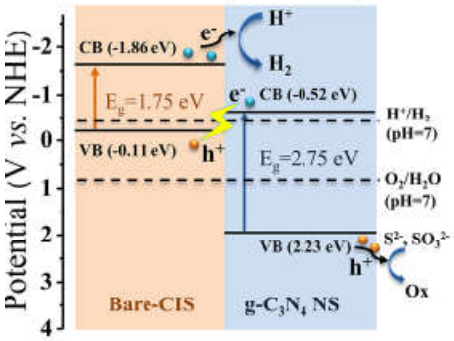

Figure 30: Electronic band structures of bare-CIS and g-C_3N_4 giving rise to a Z-scheme photocatalyst [73]

VII. ADVANTAGES OF Z-SCHEME MATERIALS FOR PHOTOELECTROCHEMICAL WATER SPLITTING

PEC water splitting is a promising solar-to-hydrogen pathway for hydrogen production at semi-central and central scales, offering the potential for high conversion efficiency at low operating temperatures using cost-effective thin-film and/or particle semiconductor materials. In PEC water splitting, various materials were utilized including metal oxides, mixed oxides, and chalcogenides etc. but the similar materials were involved in Z-scheme mechanism is a new technology for the generation of H_2 fuel through water splitting. The Z-scheme photocatalytic system can effectively overcome drawbacks of single catalyst, enhance their redox ability, photoabsorption range, and boost its charge-separation efficiency. Choosing two appropriate semiconductors to form Z-scheme photocatalysts can efficiently improve the charges transfer on the interface and also suppress separation of photoinduced electron-hole pairs. Additionally, the Z-scheme system possesses higher redox potential than that of ordinary heterojunction structure, suggesting that the Z-scheme system has a desirable reducing capacity for H_2 production. Though a lot of Z-scheme photocatalysts have been synthesized, it is also a great challenge to find a suitable strategy to prepare simple, economical, stable and highly efficient photocatalysts for H_2 production.

VIII. CONCLUSIONS

PEC water splitting is a promising route for sustainable hydrogen production. In general, three components are required for photochemical and PEC water splitting: (i) catalyst, (ii) visible-light absorber, and (iii) sacrificial electron donor. In photochemical water splitting reactions, water splitting takes place at the semiconductor electrolyte interface [75]. Moreover, at the interface between the semiconductor and liquid can be produced the necessary potential for water splitting. The semiconductor must be photostable in aqueous

solutions of different electrolytes to avoid photo-corrosion. Based on the band-edge location of the semiconducting material, they may be energetic in the production of hydrogen and oxygen to complete the water splitting reaction. Up to now, extensive efforts have been made, and significant advances have been achieved in the research on photocatalytic water splitting, including exploration of suitable materials for light harvesting, strategies for photogenerated charge separation, and efficient cocatalysts for proton reduction and water oxidation reactions. Herein, I demonstrated that the importance of PEC water splitting, affecting factors, and the classification of Z-scheme materials. It also covers the various metal oxide, metal sulfide and g-C_3N_4 based semiconductor Z-scheme materials for the generation of H_2 fuel from water slitting and its mechanisms exclusively.

REFERENCES

[1] T. Hisatomi, J. Kubota and K. Domen, Recent advances in semiconductors for photocatalytic and photoelectrochemical water splitting, Chem. Soc. Rev. 43 (2014) 7520-7535.
[2] A. Fujishima, K. Honda, Electrochemical photolysis of water at a semiconductor electrode, Nature 238(1972) 37-38.
[3] Y. Li, J.Z. Zhang, Hydrogen generation from photoelectrochemical water splitting based on nanomaterials, Laser Photonics Rev. 4 (2010) 517-528.
[4] Y.R. Steven, A.H. Jonathan, S. Kimberly, D.J. Thomas, J.E. Arthur, J.H. Joep, G.N. Daniel, Wireless solar water splitting using silicon-based semiconductors and earth-abundant catalysts, Science 334 (2011) 645-648.
[5] N.A. Kelly, T.L. Gibson, Design and characterization of a robust photoelectrochemical device to generate hydrogen using solar water splitting, Int. J. Hydrogen Energy 31 (2006) 1658-1673.
[6] L.J. Minggu, W.R.W. Daud, M.B. Kassim, An overview of photocells and photoreactors for photoelectrochemical water splitting, Int. J. Hydrogen Energy 35 (2010) 5233-5244.
[7] A. Kudo, Y. Miseki, Heterogeneous photocatalyst materials for water splitting, Chem. Soc. Rev. 38 (2009) 253-278.
[8] Q. Li, B.D. Guo, J.G. Yu, J.R. Ran, B.H. Zhang, H.J. Yan, J.R. Gong, Highly efficient visible-light-driven photocatalytic hydrogen production of CdS-cluster-decorated graphene nanosheet, J. Am. Chem. Soc. 133 (2011) 10878-10884.
[9] Y. Moriya, T. Takata, K. Domen, Recent progress in the development of (Oxy) nitride photocatalysts for water splitting under visible-light irradiation, Coordin. Chem. Rev. 257 (2013) 1957-1969.
[10] P. Zhou, J. Yu, M. Jaroniec, All-solid-state Z-scheme photocatalytic systems, Adv. Mater. 26 (2014) 4920-4935.
[11] W. Wang, M. Xu, X. Xu, W. Zhou, Z. Shao, Perovskite oxide-based electrodes for high-performance photoelectrochemical water splitting: A review, Angew. Chemie Int. Ed. (2019), DOI: 10.1002/anie.201900292
[12] H, Li, W. Tu, Y. Zhou, Z. Zou, Z-Scheme photocatalytic systems for promoting photocatalytic performance: recent progress and future challenges, Adv. Sci. 3 (2016) 1500389.
[13] A.J. Bard, Photoelectrochemistry and heterogeneous photocatalysis at semiconductors, J. Photochem. 10 (1979) 59-75.
[14] H. Tada, T. Mitsui, T. Kiyonaga, T. Akita, K. Tanaka, All-solid-state Z-scheme in CdS-Au-TiO_2 three-component nanojunction system, Nat. Mater. 5 (2006) 782-786.
[15] J.C. Wang, H.C. Yao, Z.Y. Fan, L. Zhang, J.S. Wang, S.Q. Zang, Z.J. Li, Indirect Z-scheme BiOI/g-C_3N_4 photocatalysts with enhanced photoreduction CO_2 activity under visible light irradiation, ACS Appl. Mater. Interfaces 8 (2016) 3765-3775.
[16] J. Yu, S. Wang, J. Low, W. Xiao, Enhanced photocatalytic performance of direct Z-scheme g-C_3N_4-TiO_2 photocatalysts for the decomposition of formaldehyde in air. Phys. Chem. Chem. Phys. 15 (2013)16883-16890.
[17] J. Low, C. Jiang, B. Cheng, S. Wageh, A.A. Al-Ghamdi, J. Yu, A review of direct Z-scheme photocatalysts, Small Methods 1 (2017)1700080.
[18] Q. Xu, L. Zhang, J. Yu, S. Wageh, A.A. Al-Ghamdi, M. Jaroniec, Direct Z-scheme photocatalysts: principles, synthesis, and applications, Mater. Today 21 (2018) 1042-1063.
[19] K. Maeda, Photocatalytic water splitting using semiconductor particles: history and recent developments, J. Photochem. Photobiol. C: Photochem. Rev. 12 (2011) 237-268.
[20] T. Jafari, E. Moharreri, A. Amin, R. Miao, W. Song, S. Suib, Photocatalytic water splitting-the untamed dream: a review of recent advances, Molecules 21 (2016) 900.
[21] Y. Sasaki, H. Nemoto, K. Saito, A. Kudo, Solar water splitting using powdered photocatalysts driven by Z-schematic interparticle electron transfer without an electron mediator, J. Phys. Chem. C 113 (2009) 17536-17542.
[22] K. Sayama, R. Yoshida, H. Kusama, K. Okabe, Y. Abe, H. Arakawa, Photocatalytic decomposition of water into H_2 and O_2 by a two-step photoexcitation reaction using a WO_3 suspension catalyst and an Fe^{3+}/Fe^{2+} redox system, Chem. Phys. Letters 277 (1997) 387-391.
[23] K. Sayama, K. Mukasa, R. Abe, Y. Abe, H. Arakawa, A new photocatalytic water splitting system under visible light irradiation mimicking a Z-scheme mechanism in photosynthesis, J. Photochem. Photobiol. A: Chem. 148 (2002) 71-77.
[24] K. Maeda, K. Domen, Photocatalytic water splitting: recent progress and future challenges, J. Phys. Chem. Letters 1 (2010) 2655-2661.
[25] R. Abe, Z-Scheme type water splitting into H_2 and O_2 under visible light through two-step photoexcitation between two different photocatalysts, new and future developments in catalysis, Solar Photocatalysis, 2013, 341-370.
[26] Y. Sasaki, A. Iwase, H. Kato, A. Kudo, The effect of co-catalyst for Z-scheme photocatalysis systems with an Fe^{3+}/Fe^{2+} electron mediator on overall water splitting under visible light irradiation, J. Catalysis 259 (2008) 133-137.
[27] X. Han, Q. Kuang, M. Jin, Z. Xie, L. Zheng, Synthesis of titania nanosheets with a high percentage of exposed (001) facets and related photocatalytic properties, J. Am. Chem. Soc. 131 (2009) 3152-3153.
[28] Y. Li, X. Wei, B. Zhu, H. Wang, Y. Tang, T.C. Sum, X. Chen, Hierarchically branched Fe_2O_3@TiO_2 nanorod arrays for photoelectrochemical water splitting: facile synthesis and enhanced photoelectrochemical performance, Nanoscale 8 (2016) 11284-11290.
[29] P. Peerakiatkhajohn, T. Butburee, J.H. Yun, H. Chen, R.M. Richards, L. Wang, A hybrid photoelectrode with plasmonic Au@TiO_2 nanoparticles for enhanced photoelectrochemical water splitting, J. Mater. Chem. A 3 (2015) 20127-20133.
[30] L.J. Minggu, K.H. Ng, H.A. Kadir, M.B. Kassim, Bilayer n-WO_3/p-Cu_2O photoelectrode with photocurrent enhancement in aqueous electrolyte photoelectrochemical reaction, Ceramics International 40 (2014) 16015-16021.
[31] J. Li, H. Hao, Z. Zhu, Construction of g-C_3N_4-WO_3-Bi_2WO_6 double Z-scheme system with enhanced photoelectrochemical performance, Mater. Letters 168 (2016) 180-183.
[32] J.R. Ding, K.S. Kim, 1-D WO_3@$BiVO_4$ heterojunctions with highly enhanced photoelectrochemical performance, Chem. Eng. J. 334 (2018) 1650-1656.

[33] Y. Li, J. Feng, H. Li, X. Wei, R. Wang, A. Zhou, Photoelectrochemical splitting of natural seawater with α-Fe_2O_3/WO_3 nanorod arrays, Inter. J. Hydrogen Energy 41 (2016) 4096-4105.
[34] A. Verma, A. Srivastav, S. Sharma, P. Badami, V.R. Satsangi, R. Shrivastav, A.M. Kannan, D.K. Avasthi, S. Dass, MWCNTs and Cu_2O sensitized $TiFe_2O_3$ photoanode for improved water splitting performance, Inter. J. Hydrogen Energy 43 (2018) 6049-6059.
[35] Q. Liu, D. Ding, C. Ning, X. Wang, α-Fe_2O_3/Ti–Nb–Zr–O composite photoanode for enhanced photoelectrochemical water splitting, Mater. Sci. Eng. B 196 (2015) 15-22.
[36] Z. Liu, C. Liu, J. Ya, E. Lei, Controlled synthesis of ZnO and TiO_2 nanotubes by chemical method and their application in dye-sensitized solar cells, Renew Energy 36 (2011) 1177-1181.
[37] X. Sun, Q. Li, J. Jiang, Y. Mao, Morphology-tunable synthesis of ZnO nanoforest and its photoelectrochemical performance, Nanoscale 6 (2014) 8769-8780.
[38] S. Sohila, R. Rajendran, Z. Yaakob, M. Teridi, K. Sopian, Photoelectrochemical water splitting performance of flower like ZnO nanostructures synthesized by a novel chemical method, J. Mater. Sci. Mater. Electron. 27 (2016) 2846-2851.
[39] M.F. Weber, M.J. Dignam, Splitting water with semiconducting photoelectrodes defficiency considerations, Int. J. Hydrogen Energy 11 (1986) 225-232.
[40] D. Yolacan, N.D. Sankir, Enhanced photoelectrochemical and photocatalytic properties of 3D hierarchical ZnO nanostructures, J. Alloy Comp. 726 (2017) 474-483.
[41] M. Balamurugan, G. Yun, K.S. Ahn, S.H. Kang, Revealing the beneficial effects of $FeVO_4$ nanoshell layer on the $BiVO_4$ inverse opal core layer for photoelectrochemical water oxidation, J. Phys. Chem. C 121 (2017) 7625-7634.
[42] J. Xian, D. Li, J. Chen, X. Li, M. He, Y. Shao, L. Yu, J. Fang, TiO_2 nanotube array, graphene, CdS quantum dots composite film in Z-scheme with enhanced photoactivity and photostability, ACS Appl. Mater. Interfaces 6 (2014) 13157-13166.
[43] S.K. Biswas, J.O. Baeg, Enhanced photoactivity of visible light responsive W incorporated $FeVO_4$ photoanode for solar water splitting, Int. J. Hydrogen Energy 38 (2013) 14451-14457.
[44] Z. Jiao, X. Guan, M. Wang, Q. Wang, B. Xu, Y. Bi, X.S. Zhao, Undamaged depositing large-area ZnO quantum dots/RGO films on photoelectrodes for the construction of pure Z-scheme, Chem. Eng. J. 356 (2019) 781-790.
[45] Q. Nie, L. Yang, C. Cao, Y. Zeng, G. Wang, C. Wang, S. Lin, Interface optimization of ZnO nanorod/CdS quantum dots heterostructure by a facile two-step low-temperature thermal treatment for improved photoelectrochemical water splitting, Chem. Eng. J. 325 (2017) 151-159.
[46] M. Seol, J.W. Jang, S. Cho, J.S. Lee, K. Yong, Highly efficient and stable cadmium chalcogenide quantum dot/ZnO nanowires for photoelectrochemical hydrogen generation, Chem. Mater. 25 (2013) 184-189.
[47] A. Paracchino1, V. Laporte, K. Sivula, M. Grätzel, E. Thimsen, Highly active oxide photocathode for photoelectrochemical water reduction, Nat. Mater. 10 (2011) 456-461.
[48] Y. Cong, Y. Ge, T. Zhang, Q. Wang, M. Shao, Y. Zhang, Fabrication of Z-Scheme Fe_2O_3–MoS_2–Cu_2O ternary nanofilm with significantly enhanced photoelectrocatalytic performance, Ind. Eng. Chem. Res. 57 (2018) 881-890.
[49] J.S. Yoon, J.W. Lee, Y.M. Sung, Enhanced photoelectrochemical properties of Z-scheme ZnO/pn Cu_2O PV-PEC cells, J. Alloys Compounds 771 (2019) 869-876.
[50] P. Lu, W. Zhou, Y. Li, J. Wang, P. Wu, CuO nanosheets/ZnO nanorods synthesized by a template-free hydrothermal approach and their optical and magnetic characteristics, Ceram. Int. 43 (2017) 9798-9805.
[51] X. Yin, Q. Liu, Y. Yang, Y. Liu, K. Wang, Y. Li, D. Li, X. Qiu, W. Li, J. Li, An efficient tandem photoelectrochemical cell composed of FeOOH/TiO_2/$BiVO_4$ and Cu_2O for self-driven solar water splitting, Int. J. Hydrogen Energy 44 (2019) 594-604.
[52] Z. Li, J. Liu, D. Wang, Y. Gao, J. Shen, Cu_2O/Cu/TiO_2 nanotube ohmic heterojunction arrays with enhanced photocatalytic hydrogen production activity, Int. J. Hydrogen Energy 37 (2012) 6431-6437.
[53] P.K. Dubey, R. Kumar, R.S. Tiwari, O.N. Srivastava, A.C. Pandey, P. Singh, Surface modification of aligned TiO_2 nanotubes by Cu_2O nanoparticles and their enhanced photoelectrochemical properties and hydrogen generation application, Int. J. Hydrogen Energy 43 (2018) 6867-6878.
[54] W. Fan, X. Yu, H.C. Lu, H. Bai, C. Zhang, W. Shi, Fabrication of TiO_2/RGO/Cu_2O heterostructure for photoelectrochemical hydrogen production, Appl. Catal. B Environ. 181 (2016) 7-15.
[55] Z.F. Huang, L. Pan, J.J. Zou, X. Zhang, L. Wang, Nanostructured bismuth vanadate-based materials for solar-energy-driven water oxidation: a review on recent progress, Nanoscale 6 (2014) 14044-14063.
[56] R.S. Roth, J.L. Waring, Synthesis and stability of bismutotantalite, stibiotantalite and chemically similar ABO_4 compounds, Am. Mineral. 48 (1963) 1348-1356.
[57] A. Kudo, K. Ueda, H. Kato, I. Mikami, Photocatalytic O_2 evolution under visible light irradiation on $BiVO_4$ in aqueous $AgNO_3$ solution, Catal. Lett. 53 (1998) 229-230.
[58] M. Zhu, Z. Sun, M. Fujitsuka, T. Majima, Z-scheme photocatalytic water splitting on a 2D heterostructure of black phosphorus/bismuth vanadate using visible light, Angew. Chem. Inter. Ed. 57 (2018) 2160-2164.
[59] J. Safaei, H. Ullah, N.A. Mohamed, M.F. Noh, M.F. Soh, A.A. Tahir, N.A. Ludin, M.A. Ibrahim, W.N. Isahak, M.A. Teridi, Enhanced photoelectrochemical performance of Z-scheme g-C_3N_4/$BiVO_4$ photocatalyst, Appl. Catal. B Environ. 234 (2018) 296-310.
[60] T. Soltani, A. Tayyebi, B.K. Lee, $BiFeO_3$/$BiVO_4$ p-n heterojunction for efficient and stable photocatalytic and photoelectrochemical water splitting under visible-light irradiation, Catalysis Today (2018), DOI: 10.1016/j.cattod.2018.09.030
[61] D. Ayodhys, G. Veerabhadram, Green synthesis, optical, structural, photocatalytic, fluorescence quenching and degradation studies of ZnS nanoparticles, J. Fluorescence 26 (2016) 2165-2175.
[62] M.A. Hassan, J.H. Kang, M.A. Johar, J.S. Ha, S.W. Ryu, High-performance ZnS/GaN heterostructure photoanode for photoelectrochemical water splitting applications, Acta Materialia 146 (2018) 171-175.
[63] X. Hao, J. Zhou, Z. Cui, Y. Wang, Y. Wang, Z. Zou, Zn-vacancy mediated electron-hole separation in ZnS/g-C_3N_4 heterojunction for efficient visible-light photocatalytic hydrogen production, Appl. Catal. B 229 (2018) 41-51.
[64] D. Ayodhys, G. Veerabhadram, One-pot green synthesis, characterization, photocatalytic, sensing and antimicrobial studies of Calotropis gigantea leaf extract capped CdS NPs, Mater. Sci. Eng. B 225 (2017) 33-44.
[65] T. Hu, P. Li, J. Zhang, C. Liang, K. Dai, Highly efficient direct Z-scheme WO_3/CdS-diethylenetriamine photocatalyst and its enhanced photocatalytic H_2 evolution under visible light irradiation, Appl. Surf. Sci. 442 (2018) 20-29.
[66] C.H. Li, C.W. Hsu, S.Y. Lu, TiO_2 nanocrystals decorated Z-schemed core-shell CdS-CdO nanorod arrays as high efficiency anodes for photoelectrochemical hydrogen generation, J. Colloid Interface Sci. 521 (2018) 216-225.
[67] L. Wang, Y. Tong, J. Feng, J. Hou, J. Li, X. Hou, J. Liang, G-C_3N_4-based films: A rising star for photoelectrochemical water splitting, Sustainable Mater. Technol. 17 (2018) e00089.
[68] Z. Zhao, Y. Sun, F. Dong, Graphitic carbon nitride based nanocomposites: a review, Nanoscale 7 (2014) 15-37.
[69] L. Jiang, X. Yuan, G. Zeng, Z. Wu, J. Liang, X. Chen, L. Leng, H. Wang, H. Wang, Metal-free efficient photocatalyst for stable visible-light photocatalytic degradation of refractory pollutant, Appl. Catal. B Environ. 221 (2018) 715-725.

[70] Y. Hong, Y. Jiang, C. Li, W. Fan, X. Yan, M. Yan, W. Shi, In-situ synthesis of direct solid-state Z-scheme V_2O_5/g-C_3N_4 heterojunctions with enhanced visible light efficiency in photocatalytic degradation of pollutants, Appl. Catal. B Environ. 180 (2016) 663-673.
[71] H. Su, J. Zhou, L. Miao, J. Shi, Y. Gu, P. Wang, Y. Tian, X. Mu, A. Wei, L. Huang, S. Chen, A hybrid hydrogel with protonated g-C_3N_4 and graphene oxide as an efficient absorber for solar steam evaporation, Sustainable Mater. Technol. 20 (2019) e00095.
[72] L. Jiang, X. Yuan, G. Zeng, J. Liang, X. Chen, H. Yu, H. Wang, Z. Wu, J. Zhang, T. Xiong, In-situ synthesis of direct solid-state dual Z-scheme WO_3/g-C_3N_4/Bi_2O_3 photocatalyst for the degradation of refractory pollutant, Appl. Catal. B: Environ. 227 (2018) 376-385.
[73] X. Li, K. Xie, L. Song, M. Zhao, Z. Zhang, Enhanced photocarrier separation in hierarchical graphitic-C_3N_4-supported $CuInS_2$ for noble-metal-free Z-scheme photocatalytic water splitting, ACS Appl. Mater. Interfaces 9 (2017) 24577-24583
[74] Y. Yu, S. Cheng, L. Wang, W. Zhu, L. Luo, X. Xu, F. Song, X. Li, J. Wang, Self-assembly of yolk-shell porous Fe-doped g-C3N4 microarchitectures with excellent photocatalytic performance under visible light, Sustainable Mater. Technol. 17 (2018) e00072.
[75] M. Ahmed, I. Dincer, A review on photoelectrochemical hydrogen production systems: Challenges and future directions, Int. J. Hydrogen Energy 44 (2019) 2474-2507.